TAMPEREEN TEKNILLINEN YLIOPISTO
TAMPERE UNIVERSITY OF TECHNOLOGY

JONI TOPPARI

# ACTIVE HARMONIC FILTERING WITH A STATIC SYNCHRONOUS COMPENSATOR IN HIGH VOLTAGE APPLICATIONS

Master of Science Thesis

Examiner: Assist. Prof. Tuomas Messo
Examiner and topic approved on 28 March 2018

# ABSTRACT

**JONI TOPPARI**: Active Harmonic Filtering with a Static Synchronous Compensator in High Voltage Applications
Tampere University of technology
Master of Science Thesis, 65 pages, 1 Appendix page
May 2018
Master's Degree Programme in Electrical Engineering
Major: Power Electronics
Examiner: Assistant Professor Tuomas Messo

Keywords: active harmonic filtering, harmonics, second order generalized integrator, synchronous reference frame, STATCOM

Harmonics compensation has become increasingly important as the presence of nonlinear loads and the use of power electronic devices, both generating harmonics, have increased. Harmonics increase losses and have unwanted impacts on different equipment and on the entire power system. Standards and transmission operators' specifications set limits for harmonics in the grid. Passive power filters, the traditional solution to compensate harmonics, have a number of short-comings especially under changing grid conditions. Thus, the harmonic limits are not always met. Active harmonic filters, representing newer technology, can automatically correct their tuning to varying grid and component characteristics thus providing an advanced solution to this harmonic issue gathering increasing attention.

In this thesis, two harmonics detection methods were studied: a method based on the conventional dq-theory in the synchronous reference frame (SRF) and another based on a Multiple Second Order Generalized Integrator (MSOGI) in the stationary reference frame. The developed active filter features were designed as an add-on feature on a reactive power compensation system Static Synchronous Compensator (STATCOM). The operation principles and theory behind these harmonics detection methods were studied comprehensively. Methods for positive and negative sequence extraction as well as grid synchronization were also considered. Moreover, the suitability of the studied methods to be used in a full-scale Modular Multilevel Converter (MMC) based STATCOM system was considered. Simulations for the studied methods were performed in PSCAD environment in order to demonstrate and compare their feasibilities in a steady-state operation.

According to the simulation results, both methods were able to compensate selected harmonics completely in STATCOM's maximum capacitive, maximum inductive and zero-operation points. Compensation of positive and negative sequence harmonics worked similarly and neither of the methods significantly strengthened individual uncontrolled grid harmonics. The structure of the MSOGI based method appeared to be slightly more complex and the control implementation in MSOGI's stationary reference frame was considered much more challenging than corresponding control in the conventional synchronous reference frame (SRF based method). On the other hand, the suitability of the MSOGI based active filter method for both three-phase and single-phase applications was found superior compared to the studied SRF based method, which in turn is only suitable for three-phase applications.

# TIIVISTELMÄ

**JONI TOPPARI**: Harmonisten aktiivisuodatus STATCOMilla suurjännitesovelluksissa
Tampereen teknillinen yliopisto
Diplomityö, 65 sivua, 1 liitesivu
Toukokuu 2018
Sähkötekniikan diplomi-insinöörin tutkinto-ohjelma
Pääaine: Tehoelektroniikka
Tarkastaja: apulaisprofessori Tuomas Messo

Avainsanat: aktiivisuodin, harmoniset, second order generalized integrator, synchronous reference frame, STATCOM

Harmonisten yliaaltojen kompensoinnista on tullut entistä tärkeämpää, koska yliaaltoja tuottavien epälineaaristen kuormien sekä tehoelektroniikkalaitteiden käyttö on lisääntynyt. Harmoniset yliaallot kasvattavat häviöitä ja niillä on haitallinen vaikutus sekä moniin sähkölaitteisiin että koko sähköjärjestelmään. Näiden vaikutusten rajoittamiseksi standardeissa sekä sähköverkkoyhtiöiden spesifikaatioissa on asetettu rajoituksia harmonisten sallituille määrille. Perinteinen ratkaisu harmonisten kompensoimiseen passiivisuotimilla sisältää monia puutteita erityisesti verkon muutostilanteissa, minkä seurauksena asetettuja harmonisten rajoja ei aina saavuteta. Aktiivisuotimet edustavat uudempaa teknologiaa ja ne mukautuvat automaattisesti verkon sekä laitekompontenttien muutoksiin tarjoten näin edistyksellisemmän ratkaisun harmonisten yliaaltojen ongelmaan.

Tässä diplomityössä tutkittiin kahta harmonisten tunnistusmetodia: toinen perustuen dq-teoriaan ja synchronous reference frame (SRF) -tasoon sekä toinen perustuen Multiple Second Order Generalized Integrator (MSOGI) -rakenteeseen ja stationary reference frame -tasoon. Toteutetut aktiivisuodinominasuudet suunniteltiin loistehon kompensointijärjestelmä STATCOMin lisäominaisuudeksi. Harmonisten tunnistusmetodien teoria ja toimintaperiaatteet tutkittiin kokonaisvaltaisesti. Myös tavat harmonisten positiivisten ja negatiivisten sekvenssien tunnistamiseen sekä verkkosynkronointiin huomioitiin. Lisäksi tutkittujen metodien sopivuutta käytettäväksi täysimittaisessa Modular Multilevel Converter STATCOMissa tarkasteltiin. Simuloinnit metodien toimintakyvyn demonstroimiseksi ja vertailemiseksi suoritettiin PSCAD ympäristössä.

Simulointituloksien perusteella molemmat metodit kykenivät kompensoimaan määritetyt harmoniset kokonaan STATCOMin maksimikapasitiivisessa, maksimi-induktiivisessa sekä nollatoimintapisteissä. Positiivisten ja negatiivisten sekvenssien kompensointi toimi samalla tavalla eikä kumpikaan tutkituista metodeista vahvistanut merkittävästi yksittäisiä kontrolloimattomia harmonisia. MSOGIn rakenne oli monimutkaisempi ja säädön toteuttaminen MSOGIn stationary reference frame -tasossa havaittiin olevan merkittävästi haasteellisempaa kuin vastaavan säädön toteutus perinteisessä synchronous reference frame -tasossa (SRF-tason metodi). Toisaalta MSOGIn soveltuvuus käytettäväksi sekä kolmivaiheisissa että yksivaiheisissa järjestelmissä todettiin merkittäväksi eduksi verrattuna SRF-tason metodiin, joka puolestaan soveltuu vain kolmivaiheisiin sovelluksiin.

# PREFACE

This Master of Science Thesis was written for GE Grid Solutions Oy between September 2017 and May 2018.

MSc. Pasi Vuorenpää within the company served as the instructor of the work offering very good comments which improved the quality of the work considerably. Also, MSc. Sami Kuusinen and Ph.D. Anssi Mäkinen offered great guidance whenever needed. Jani Honkanen was writing his thesis simultaneously within the company of a subject related closely to mine. Sharing thoughts with him helped me to overcome many issues. I would like to thank all of them for the great help and support along this work.

Moreover, I would like to thank MSc. Vesa Oinonen for offering me this position and organizing the whole thesis process as well as Assistant Professor Tuomas Messo for examining my thesis. In addition, I want to thank all my colleagues along with everyone else who in one way or another took part in this work. Furthermore, I am especially grateful to my family for the invaluable support and motivation during all my studies.

Tampere, 25.4.2018

Joni Toppari

# CONTENTS

# APPENDIX A: SYSTEM PARAMETERS FOR SIMULATIONS

# LIST OF SYMBOLS AND ABBREVIATIONS

| | |
|---|---|
| AC | Alternating Current |
| DC | Direct Current |
| DDSRF | Decoupled Double Synchronous Reference Frame |
| DSOGI | Double Second Order Generalized Integrator |
| FACTS | Flexible AC Transmission Systems |
| FLL | Frequency Locked Loop |
| GTO | Gate Turn-Off Thyristor |
| HVDC | High Voltage Direct Current |
| IGBT | Insulated Gate Bipolar Transistor |
| MDSOGI | Multiple Double Second Order Generalized Integrator |
| MMC | Modular Multilevel Converter |
| MSOGI | Multiple Second Order Generalized Integrator |
| PCC | Point of Common Coupling |
| PLL | Phase Locked Loop |
| PNSC | Positive Negative Sequence Calculator |
| PWM | Pulse Width Modulation |
| SOGI | Second Order Generalized Integrator |
| SRF | Synchronous Reference Frame |
| SVC | Static Var Compensator |
| STATCOM | Static Synchronous Compensator |
| THD | Total harmonic distortion |
| VSC | Voltage Source Converter |

| | |
|---|---|
| $a$ | A phase shift of 120 degrees |
| $D$ | Distortion power |
| $h$ | Order of the harmonic component |
| $I_1$ | Fundamental current RMS value |
| $I_h$ | Current harmonic component $h$ RMS value |
| $I_P$ | Active current |
| $I_Q$ | Reactive current |
| $k$ | SOGI gain |
| $k_c$ | Active power capacity increase factor |
| $k_{PV}$ | Losses reduction factor |
| $n$ | Number of submodules in series |
| $P$ | Active power |
| $P_a$ | Losses due to active power |
| $P_r$ | Losses due to reactive power |
| $P_l$ | Thermal power losses |
| $Q$ | Reactive power |
| $q$ | 90 degrees phase shift |
| $qv'$ | SOGI's inquadrature output signal |
| $R$ | Resistance |
| $S$ | Apparent power |
| $U$ | Magnitude of the voltage vector in synchronous reference frame |
| $U_d$ | Pure DC component of the voltage d component |
| $U_q$ | Pure DC component of the voltage q component |
| $v$ | Instantaneous voltage signal |
| $v'$ | SOGI's instantaneous output voltage |

| | |
|---|---|
| $V_1$ | Fundamental voltage RMS value |
| $\boldsymbol{v}_{abc}$ | A three-phase voltage vector in natural reference frame |
| $\boldsymbol{v}_{\alpha\beta}$ | Voltage vector in αβ-frame |
| $\boldsymbol{v}_{\alpha\beta,rotated}$ | Rotated voltage vector in αβ-frame |
| $V_a$ | Phase A voltage phasor |
| $V_{AB1}$ | Primary side line-to-line voltage between phases A and B |
| $V_{ab1}$ | Secondary side line-to-line voltage between phases A and B |
| $V_{AN1}$ | Primary side phase A voltage |
| $V_b$ | Phase B voltage phasor |
| $V_{BC1}$ | Primary side line-to-line voltage between phases B and C |
| $V_{bc1}$ | Secondary side line-to-line voltage between phases B and C |
| $V_{BN1}$ | Primary side phase B voltage |
| $V_c$ | Phase C voltage phasor |
| $V_{CA1}$ | Primary side line-to-line voltage between phases C and A |
| $V_{ca1}$ | Secondary side line-to-line voltage between phases C and A |
| $V_{CN1}$ | Primary side phase C voltage |
| $v_d$ | Voltage d component |
| $v_{dh}$ | Harmonic oscillation in voltage d component |
| $\boldsymbol{v}_{dq}$ | Voltage vector in synchronous reference frame |
| $V_{GRID}$ | Grid voltage |
| $V_h$ | Voltage harmonic component $h$ RMS value |
| $V_{LL}$ | Line-to-line voltage |
| $V_{n1}$ | Voltage at the sending end |
| $V_{n2}$ | Voltage at the receiving end |
| $V_{PCC}$ | Voltage at the point of common coupling |
| $v_q$ | Voltage q component |
| $v_{qh}$ | Harmonic oscillation in voltage q component |
| $V_{VSC}$ | Voltage produced by VSC |
| $X$ | Reactance |
| $X_L$ | Line reactance |
| $Z_{GRID}$ | Grid impedance |
| | |
| $\gamma$ | FLL gain |
| $\delta$ | Phase difference between $V_{n1}$ and $V_{n2}$ |
| $\varepsilon_f$ | Frequency error variable |
| $\varepsilon_v$ | SOGI's error signal |
| $\theta$ | Rotation angle |
| $\theta_{sync}$ | Synchronization angle |
| $\varphi$ | Initial angle of the voltage vector |
| $\varphi_a$ | Initial power factor angle |
| $\varphi_b$ | Final power factor angle |
| $\varphi_1$ | Phase difference between voltage and current waveforms |
| $\omega$ | Angular frequency |
| $\omega'$ | SOGI's resonance frequency |
| $\omega_f$ | Cut-off frequency of the low-pass filter |
| $\omega_{ff}$ | FLL feedforward |
| $\omega_{sync}$ | PLL angular synchronization frequency |

# 1. INTRODUCTION

The increasing use of power electronic devices and other nonlinear loads has thrown a tremendous challenge for power system operators to maintain the good power quality in power systems [1]. Harmonic currents and voltages injected by these nonlinear loads increase losses, decrease the overall system performance and can have a harmful impact on the entire system if not addressed properly. Due to this, it has become necessary to limit these harmonics' impacts by compensating substantial grid harmonics. Consequently, various standards have been published to limit the level of distortion in power systems.

To reduce the harmonic content in power systems, several harmonics mitigation techniques have been developed. A traditional method to solve the problem of harmonic pollution has been to install passive power filters, consisting of tuned circuits of passive components such as inductors and capacitors, to absorb harmonic currents from the grid. However, these passive power filters have a number of shortcomings especially under changing grid conditions. As a result, more complex techniques have been designed to respond better to harmonic standards as well as enabling better adaptation to project specific requirements. Active power filters represent newer technology in the field of harmonics mitigation. [2]

As the electricity demand continues to grow, reactive power compensation has become more and more important by enabling maximization of the active power transmission capacity of the grid. Static Synchronous Compensator (STATCOM) is a modern reactive power compensation solution consisting of a voltage source converter, reactor and a step-down transformer. [3] The purpose of this thesis is to study possibilities for active harmonic filtering as an add-on feature on a Modular Multilevel Converter (MMC) based STATCOM system. Active harmonic filters done by two-level and three-level topologies on low voltage application are common but active harmonic filters on high voltage side can be considered a more novel example of active filtering [2, 4]. Correspondingly, regardless of the number of works published concerning MMC in the fields of Flexible AC Transmission Systems (FACTS) and High Voltage Direct Current (HVDC), the operation of MMC as an active power filter in high voltage applications isn't well-covered. [4] In this thesis, two harmonics detection methods are studied and compared comprehensively. Moreover, their feasibilities in harmonics compensation as a part of the normal operation of a full-scale MMC STATCOM are further simulated in PSCAD environment.

In chapter 2, basic theory of harmonics, their effects and a review of harmonic standards are presented. In chapter 3, fundamentals of reactive power compensation are described. Moreover, the structure and operation principle of the MMC based STATCOM system

are presented. The chosen harmonics detection methods with grid synchronization features are presented in chapter 4 which thus can be considered as the core chapter of this thesis. In chapter 5, the studied techniques are simulated in PSCAD environment to demonstrate their feasibilities. Chapter 6 provides an analysis and comparison of the studied two methods based mainly on chapters 4 and 5. Chapter 7 proposes possible future study needs to further develop the active harmonic filter feature. Finally, the last chapter sums up the entire thesis and provides final conclusions from the results.

# 2. HARMONICS

Harmonic distortion is one of the most important issues in today's power systems. In this chapter, the basic theory and phenomena related to power system harmonics are presented. Moreover, in the last subchapter important standards defining allowed harmonic distortion levels are presented briefly.

## 2.1 Basics of harmonic theory

In an ideal case, a power system consists of ideal power generators and linear loads. Under these circumstances, currents and voltages will be in shape of an ideal sine wave with a specified voltage magnitude and a constant frequency. However, for a number of reasons these conditions are not fulfilled in practice which leads to distorted current and voltage waveforms often expressed as harmonic distortion.

A linear load in an electric power system draws current which is proportional to the applied voltage. Hence the voltage waveform equals to the current waveform. Typical linear loads are for example heaters, incandescent lamps and motors. In turn, on a nonlinear load the shape of current waveform is not the same with the voltage waveform. Impedance of a nonlinear load changes with the applied voltage resulting in non-sinusoidal current drawn by the load. [5] Standard IEEE 519 defines nonlinear load as a load that draws a non-sinusoidal current wave when supplied by a sinusoidal voltage source [6]. Nonlinear loads thus lead to harmonic distortion. Rectifiers, adjustable speed motor drives and ferromagnetic devices are typical examples of nonlinear loads.

According to Fourier theorem, all non-sinusoidal periodic signals can be represented as a sum of simple sinewaves [7]. Regardless of how complex the signal is, when analyzed through the Fourier series analysis it is possible to deconstruct the signal into a series of simple sinusoids. This means that even highly distorted currents and voltages of the power system can be decomposed of the fundamental signal and possibly an infinite set of sinusoidal terms whose frequencies are integer multiplies of the fundamental frequency. These multiplies are called harmonics. Figure 1 shows a distorted total current and its decomposition.

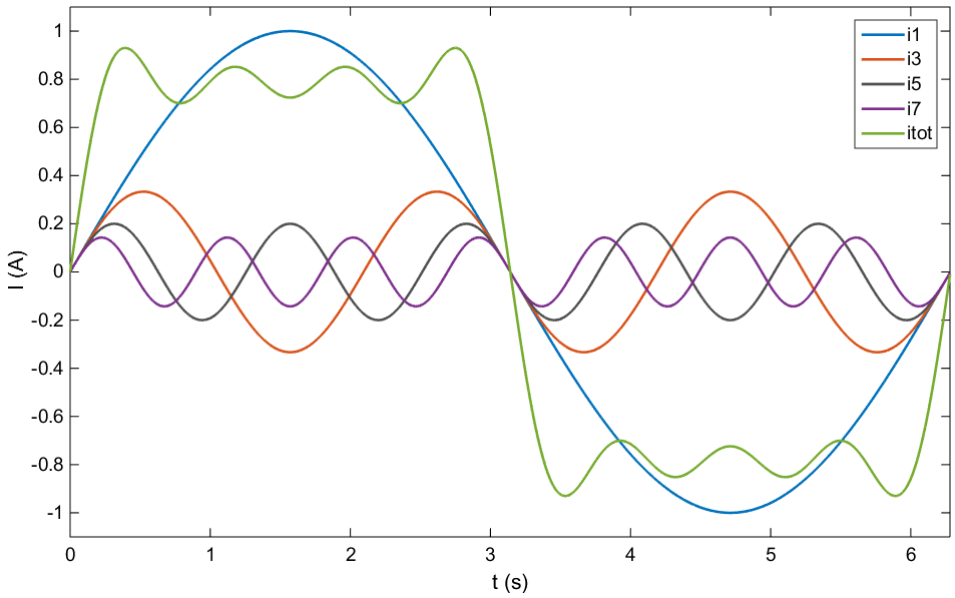


***Figure 1.*** *Distorted waveform decomposed into fundamental signal and harmonics.*

As can be seen in Figure 1, the distorted total current is composed of the fundamental frequency current and harmonic currents of 3$^{rd}$, 5$^{th}$ and 7$^{th}$ order. According to standard IEEE 519 a harmonic can be defined as a sinusoidal component of a periodic wave or quantity having a frequency that is an integral multiple of the fundamental frequency [6].

Devices causing harmonics are present in all industrial, commercial and residential installations. The problem of distorted waveforms in power systems is thus not a new phenomenon. However, the increasing number of highly nonlinear loads such as power electronic devices have created a growing concern for this issue nowadays.

## 2.2 Sources of harmonics

There exist plenty of harmonics sources especially in industrial power systems. A common characteristic for all these sources is a nonlinear voltage-current operating relationship. Any device that alters the pure sinusoidal waveform of currents or voltages is considered as a harmonic source.

Ideally, an AC generator produces pure sinusoidal voltage waveform at a fundamental frequency without any harmonics. This is the case only if generator's structure and operation are theoretically perfect i.e. windings are evenly and finely distributed and magnetic field is uniform. However, generators are not ideal in practice but have many flaws which result in non-sinusoidal voltage generation and thus harmonics supply to the grid. For example, variation in generator's airgap, non-ideal winding types and asymmetrical structure overall induce voltage distortion. This distortion level at the supply end is not significant but it still exists. In other words, harmonics are there even if all loads were linear and ideal. [8]

Nowadays, there exist numerous different situations where harmonics are generated. The greatest majority of harmonic sources can be considered to origin from power converters that use solid-state switching devices. These are for example rectifiers, inverters, voltage controllers, frequency converters and variable frequency drives. Overall nowadays increasing use of power semiconductor devices create waveforms rich in harmonics. Power converters, transformers and rotating machines can be considered as traditional sources of harmonics. Other fundamental harmonics sources are for example arc-furnaces, fluorescent lightning and other network's nonlinear loads. [1, 7]

In the future the issue of harmonics will be even more challenging as the harmonic sources will become diverse and more numerous. Especially the use of distributed generation (photovoltaics and wind power) is estimated to play a significant role in power generation in the future and will thus create challenges concerning power system harmonics. Also, the potential large-scale use of electric vehicles, which draw a significant amount of energy when charged, can significantly increase harmonics generation. Moreover, the increasing use of sensitive electronics will worsen the situation. [1, 7]

## 2.3 Effects of harmonics

The effects of harmonics distortion on different equipment vary extensively. Different machines and equipment respond differently to harmonics incidence depending on the characteristics of the equipment and the method of operation. For instance, conventional electric heating machines, stoves and incandescent lamps are basically immune to any harmonics distortion. On the other hand, in many cases harmonics may cause shortening of lifetime, increased losses and even malfunctioning in some electronic devices.

One of the main problems with harmonics is simply increased current in the system. Unwanted distortion can increase conductor's current resulting in increase of thermal losses and in the worst-case tripping of protection. Nowadays, operation of various devices depends on accurate magnitude and shape of the voltage waveform. Harmonics lead to incorrect magnitude values and distorted wave shape, which therefore may cause malfunctioning of equipment. For example, some measuring and protective instruments are prone to error under harmonics influence. [9] Moreover, possible parallel or series resonance in the system can cause amplification of harmonics and thus lead to even more problematic conditions for electric devices. In general, higher harmonics force the system to operate outside its normal specifications, which naturally leads to higher energy consumption and challenges in maintaining the normal operation. [10]

Since harmonics are of higher frequency compared to the fundamental component they tend to avoid flowing through the center of a solid conductor. In other words, they flow mainly near the conductor's surface thus reducing the effective cross-sectional area of the conductor. This leads to lower conductivity and higher losses since conductor's cross-

sectional area available to carry electron flow is not used effectively. As a result, harmonics flow between the outer edge and so-called skin depth. The higher the frequency of a harmonic is, the smaller the skin depth and thus the greater resistance of the conductor, respectively. [11] This phenomenon is known as skin effect and it can be considered as a substantial issue increasing losses in many applications.

In addition to earlier, increased eddy current losses due to harmonics are a major issue especially when considering for example transformers and motors. Whereas copper losses are directly proportional to the resistance and the square of the load current, eddy current losses are directly proportional to the square of the product of current and its corresponding frequency. Increased losses due to skin effect and higher eddy current losses may together lead to overheating of windings in motors and transformers, cause thermal insulation loss due to heating and thus lead to premature ageing and reduction in performance. [7, 10, 12]

In a four-wire three-phase system harmonic currents may have a significant impact on the neutral conductor. Under normal conditions, balanced phase currents cancel out each other in the neutral conductor i.e. there is no current flowing through the neutral. However, when the system is not entirely balanced, unbalanced currents circulate through the neutral conductor. Moreover, under highly distorted circumstances harmonics zero sequence currents add in phase in the neutral conductor. The circulation of these zero sequence harmonics in addition to the circulation of the fundamental frequency unbalanced currents may lead to neutral conductor overloading. As the neutral conductor is usually sized the same as phase conductors, dangerous overheating may occur. [1]

Overall, harmonics can have numerous harmful impacts which generally can be categorized into long-term and short-term effects. Long-term effects are mainly of thermal nature whereas short-term effects are failures and malfunctions of devices. Harmonics can furthermore go unnoticed for long periods of time if not detected properly. If harmonics are not controlled appropriately they can for example increase temperatures, lead to reduction in equipment's service life, cause damage to parts of the entire power system and thus create additional costs for the power system operator.

## 2.4 Harmonics analysis and THD

Harmonics analysis can be carried out in frequency domain instead of presenting current and voltage harmonics in time domain. The frequency domain presentation shows how much of the original signal lies within each given frequency band over a range of frequencies. The time domain representation in turn shows how the signal varies within time and gives thus more information about the real-time characteristics of the signal. As mentioned earlier, with Fourier's transform signals can be converted from time domain to frequency domain. Usually the outcome is presented in a bar chart as shown in Figure 2.

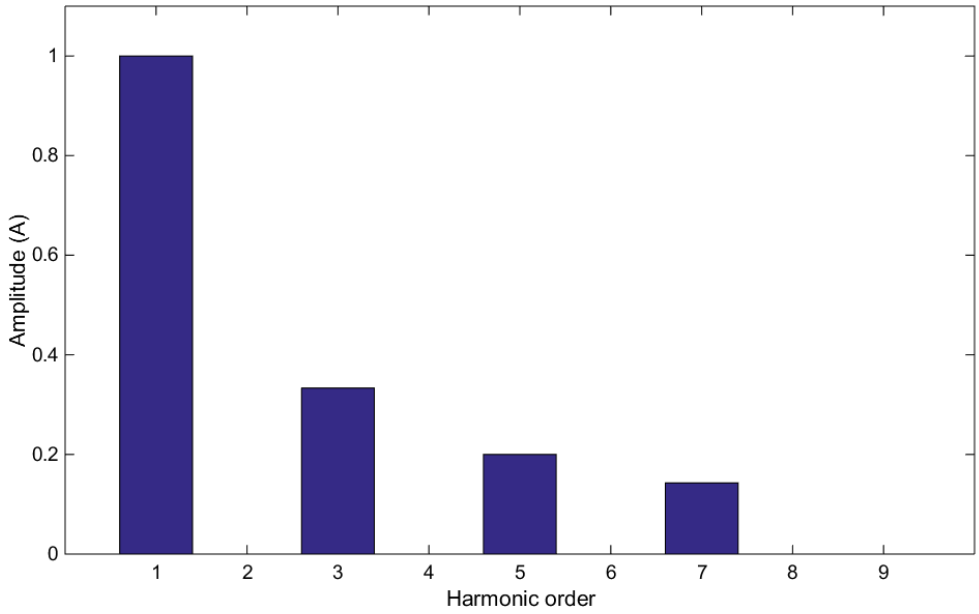


***Figure 2.*** *Distorted current waveform presented in a bar chart.*

Figure 2 presents the same current waves in a bar chart as were presented earlier in time domain in Figure 1. The first bar presents the fundamental frequency and the rest of the bars present harmonics, respectively. As can be seen, in the frequency domain representation, it can be easily noticed which harmonics occur in the original signal and in what scale. The analysis of harmonics is preferable to carry out in frequency domain. [1]

Total harmonics level in voltage and current waveforms needs to be estimated. This is necessary in order to implement proper means to mitigate harmonics in power systems and to prevent harmonics' negative influence on power system equipment. Distortion of a waveform in relation to ideal pure sine wave is analyzed by total harmonic distortion (THD). The total harmonic distortion is defined as a ratio of a sum of all harmonics components to the fundamental component of the signal. [1] For instance, total harmonic distortion for current is defined as follows:

$$THD = \frac{\sqrt{\sum_{h=2}^{\infty} I_h^2}}{I_1}, \tag{1}$$

where $I_1$ is the fundamental current RMS value and $I_n$ is the current RMS value of a corresponding harmonic order $h$. For voltage, the total harmonic distortion can be defined according to equation (2), respectively.

$$THD = \frac{\sqrt{\sum_{h=2}^{\infty} V_h^2}}{V_1} \tag{2}$$

In equation 2, $V_1$ is the fundamental voltage RMS value and $V_n$ the voltage RMS value of a corresponding harmonic order $h$ analogically to equation 1. In general, the less the particular signal looks like a pure sine wave, the stronger the harmonic content in it is and

the greater THD value it has. Therefore, THD should be minimized to maintain the quality of electricity in electric power systems; ideal pure sine wave has zero distortion level i.e. THD = 0 %. Lower THD in power systems means higher efficiency, higher power factor and lower peak currents. Different standards and regulations also define limits for harmonics distortion under which all harmonics should be kept. [1]

## 2.5 Harmonics mitigation methods

As mentioned earlier, electrical harmonic pollution is necessary to be minimized in order to keep electric networks and the whole power system safe and efficient. Harmonics can be filtered with different components and techniques of which the most important ones are passive and active filters.

Passive filters consist of passive components such as capacitors, inductors and resistors. Tuning of the filters are done by combining these passive components thus allowing filters with specific characteristics. Passive filters can be connected either in series or in parallel with the load. The existing harmonic filtering is nearly entirely based on parallel type of filters and although series configuration is also possible it is more common to connect passive filters in parallel. [13] The main idea of parallel passive filters is to create a low-impedance path from the electric network to ground for a predefined harmonic signal. This way the harmonic passes to the ground through the passive filter and does not spread to the rest of the electric network. Passive filters have a special frequency where the impedance of the filter approaches zero or respectively infinity in case of series type of passive filters. This frequency is known as resonance frequency. Designing of the filter is done so that its resonance frequency meets the frequency of a predefined harmonic. Thus, for parallel connected filters, the filter is tuned in a way that its impedance approaches zero around the harmonic frequency. In contrast, with series type of passive filters, the filter should present high impedance for the predefined harmonic frequency that needs to be blocked. [2]

The main drawback with passive filters is that they are capable of filtering only predefined harmonics. Also, if harmonic's characteristics vary, for example frequency fluctuates, the passive filter is immediately detuned and can't filter out the specific harmonic efficiently anymore. In other words, if filters were capable to automatically correct tuning due to varying characteristics such as frequency variation and component deviation, a significant advantage would be obtained. [13] Active filters are the solution for this issue since they can filter several harmonics and continuously adjust tuning to cancel out varying harmonics. Similar with passive filters, active filters can also be connected either in parallel or in series. Thus, they are categorized into shunt active filters and series active filters based on their circuit configurations. However, as it was with passive filters also shunt type of active filters are more common over series type of active filters. The main idea of active filters is to produce a waveform to the grid with the same magnitude but with 180 degrees shifted phase compared to the detected harmonic signal. Thus, the harmonic in the grid

will be canceled out. In order to work properly, active filters need to detect harmonic's frequency, magnitude and phase in the grid. After detecting the harmonic, active filters sync and inject the created waveform with opposite phase angle to the grid so that the original grid harmonic will finally be canceled out. Active filters have many advantages compared to traditional passive filters but so far the cost has still been higher. [2, 13]

## 2.6 Regulations and standards

There are several different standards and regulations defined regarding harmonic pollution in power systems. The purpose of these regulations is to ensure proper operation of the network and connected equipment by preventing harmonic distortion to exceed permissible levels. According to standard IEEE 519 harmonic distortion limits are provided to reduce the potential negative effects on user and system equipment [6]. Overall these standards determine the compatibility between distribution networks and connected devices. The main idea is that the harmonics caused by a device must not disturb the distribution networks and on the other hand each device must be capable of operating normally in the presence of disturbances up to a specific level. There are both international standards such as IEEE 519 and IEC 61000-2-4 as well as national standards for example G5/3 and G5/4 for United Kingdom. [14] In addition to these international and national standards, there may also be project-specific limits for harmonics generation and harmonics effects.

Currently, most of the countries use limits for harmonics based on international standards. Widely recognized international standards are for example IEEE 519, IEC 61000-3-6, IEC 61000-2-2, IEC 61000-2-12 and the European standard EN 50160. As not only the existence of different harmonic components but also the combination of these harmonics matters, these standards usually give harmonics limits in terms of individual harmonic component values but also as total harmonic distortion. Table 1 gives a comparison of different limits defined in above mentioned standards. The limits are given only for the odd harmonic orders.

***Table 1.*** *Limits for odd order harmonic voltages defined in well-known standards [14].*

| Standard | EN 50160 | IEEE 519 up to 69 kV | IEC 61000-2-2 IEC 61000-2-12 | IEC 61000-3-6 |
|---|---|---|---|---|
| Purpose | limits | limits | compatibility levels | indicative planning levels |
| Voltage level | LV and MV | LV and MV | LV and MV | MV |
| $h$ | Harmonic voltage as a percentage of the fundamental [%] | | | |
| 3 | 5 | 3 | 5 | 4 |
| 5 | 6 | 3 | 6 | 5 |
| 7 | 5 | 3 | 5 | 4 |
| 9 | 1.5 | 3 | 1.5 | 1.2 |
| 11 | 3.5 | 3 | 3.5 | 3 |
| 13 | 3 | 3 | 3 | 2.5 |
| 15 | 0.5 | 3 | 0.4 | 0.3 |
| 17 | 2 | 3 | 2 | 1.7 |
| 19 | 1.5 | 3 | 1.76 | 1.5 |
| 21 | 0.5 | 3 | 0.3 | 0.2 |
| 23 | 1.5 | 3 | 1.41 | 1.2 |
| 25 | 1.5 | 3 | 1.27 | 1.09 |
| $25 < h \leq 40$ | - | 3 | $2.27 \cdot (17/h) - 0.27$ | $1.9 \cdot (17/h) - 0.2$ |
| THD [%] | 8 | 5 | 8 | 6.5 |

As can be seen, different standards give mostly comparable but slightly differing limits for harmonic distortion. Giving limits in terms of voltage distortion is the ruling way to determine harmonic distortion. Usually, given limits are meant to be covered in long-term allowing thus some flexibility for short time exceeding of limits. For example, a common definition is that weekly 95 % of the short time (10 mins) harmonics should be less than given limits. Also, 99 % of harmonics over very short periods (3 seconds) should be less than given values multiplied by a factor defined differently in different standards. These definitions apply for example to standards IEEE 519 and IEC 61000-3-6. As standards allow short time exceeding of the given limits, the dynamic performance of harmonics compensation isn't that crucial. Overall, there exists a countless number of different guidelines that cover slightly different parts of the possible harmonic distortion situations. [14]

In this thesis, standard IEC 61000-3-6 is applied further when defining background distortion for simulations. IEC 61000-3-6 gives indicative planning levels which are mainly stricter compared to other standards' limits as can also be noticed in Table 1. This is because the indicative planning levels are internal quality objectives that give a safety margin thus allowing possible future connection of additional loads without exceeding the actual compatibility levels. [15] Table 2 presents the indicative planning levels for voltage harmonics up to $50^{th}$ harmonic order.

***Table 2.*** *IEC 61000-3-6 indicative voltage harmonic planning levels. Table adapted from table in [15].*

| Odd harmonics non-multiple of 3 | | Odd harmonics multiple of 3 | | Even harmonics | |
|---|---|---|---|---|---|
| Harmonic order h | Harmonic voltage % | Harmonic order h | Harmonic voltage % | Harmonic order h | Harmonic voltage % |
| 5 | 2 | 3 | 2 | 2 | 1.4 |
| 7 | 2 | 9 | 1 | 4 | 0.8 |
| 11 | 1.5 | 15 | 0.3 | 6 | 0.4 |
| 13 | 1.5 | 21 | 0.2 | 8 | 0.4 |
| $17 \leq h \leq 49$ | $1.2 \cdot 17/h$ | $21 < h \leq 45$ | 0.2 | $10 \leq h \leq 50$ | $0.19 \cdot 10/h+0.16$ |

The indicative voltage harmonic planning levels given in Table 2 are for high voltage and extra-high voltage systems (> 35 kV) whereas in Table 1 the values are given for medium voltage systems. Therefore, limits defined by IEC 61000-3-6 in Table 1 and Table 2 are different. The voltage THD limit for high voltage systems is 3 % instead of 6.5 % that is defined for medium voltage system in Table 1. [15] In this thesis, IEC 61000-3-6 for high voltage systems is applied.

# 3. REACTIVE POWER COMPENSATION

Reactive power compensation has become increasingly important as it affects the operational, economical and quality of the service aspects in electric power systems. In this chapter, basics of reactive power compensation are presented. Moreover, the last subchapter presents the main structure and operation principle of the STATCOM system in which the active harmonic filtering is to be implemented.

## 3.1 Need for reactive power compensation

Active, reactive and apparent powers are fundamental concepts regarding classical single-phase and three-phase AC systems. In a linear system, current and voltage are both sinusoidal and in the same phase if the load is purely resistive. The product of current and voltage is thus always positive resulting in positive power. This means that energy is transferred from source to load and furthermore the flow is unidirectional. This power is useful power and often referred as real power or active power $P$. On the other hand, if the load is purely reactive, i.e. capacitive or inductive, the phase difference $\varphi_1$ between voltage and current is 90 degrees and thus the product of current and voltage is positive during two quarters and negative during the other two quarters of the cycle. This means that energy transferred to the load is as much as energy coming back from the load. In other words, energy flows back and forth between the source and the load resulting in zero average power. [16] This power is often referred as reactive power $Q$. Calculations of active and reactive powers as well as their relationship to apparent power $S$ are presented in equations 3–5.

$$P = V\,I\cos\varphi_1 \tag{3}$$

$$Q = VI\sin\varphi_1 \tag{4}$$

$$S = \sqrt{P^2 + Q^2} \tag{5}$$

In equations 3–5, $V$ is the RMS phase voltage, $I$ is the RMS current of one phase and $\varphi_1$ is the phase difference between the phase voltage and current. The calculated powers are single-phase powers. Usually, these powers are calculated from fundamental voltage and current values. If harmonics are present, their effect can be expressed with the help of an additional power called distortion power $D$. Moreover, the ratio of active power $P$ to apparent power $S$ is referred as power factor $\cos\varphi_1$ which is considered as an important power quality measure. Power factor equals one when all the power is active power and zero when all the power is reactive power, respectively.

All real equipment in the power system either generate or consume reactive power and both active and reactive powers are needed for the electric network to function properly.

In practice, reactive power naturally increases losses as energy travelling between the source and the load loses its energy due to for example line resistances. Reactive power would therefore be beneficial to be created near the load where needed rather than drawing it through the grid.

One of the main issues with the transmission of reactive power is the increased current and thus increased thermal losses along transmission and distribution lines. The power losses due to line impedance are proportional to the square of the line current and are determined in a three-phase system as follows:

$$P_l = 3\, I^2 R, \tag{6}$$

where $R$ is resistance of the conductor and $I$ is the line current. By reducing reactive power transfer, smaller currents flow through the lines and thus thermal losses can be reduced radically. [17] To further illustrate the importance of the reactive power compensation, the relationship between thermal losses and the power factor $\cos\varphi_1$ can be derived as shown in the following equation:

$$P_l = 3\, I^2 R = \frac{S^2 R}{V_{LL}^2} = \frac{P^2 R}{V_{LL}^2 \cdot (\cos\varphi_1)^2} = \frac{P^2 R}{V_{LL}^2} + \frac{Q^2 R}{V_{LL}^2}, \tag{7}$$

where $R$ is the resistance of the network component for example resistance of the conductor, $I$, $S$, $P$ and $Q$ are the current, total power, active power and reactive power flowing through the network component, $V_{\mathrm{LL}}$ is line-to-line voltage and $\cos\varphi_1$ is the power factor. As can be seen, losses are inversely proportional to the square of the power factor $\cos\varphi_1$. If power factor is improved from $\cos\varphi_a$ to $\cos\varphi_b$ losses are reduced in turn by a factor of $k_{\mathrm{PV}}$.

$$k_{PV} = 1 - \left(\frac{\cos\varphi_a}{\cos\varphi_b}\right)^2 \tag{8}$$

In equation 7, this relationship is further derived into form where active power part and reactive power part of the losses are easily found. Figure 3 illustrates the relationship between losses and the power factor.

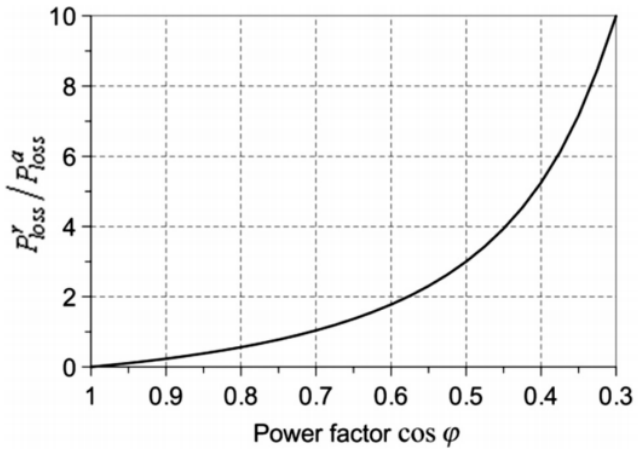


***Figure 3.*** *Relationship between power factor and the ratio of losses caused by reactive power flow to losses caused by active power flow [18].*

In Figure 3, $P_r$ represents losses due to reactive power flow and $P_a$ losses due to active power flow, respectively. It can be noticed that the power factor reaches the unity value only if the part of losses due to reactive power flow becomes zero. Improved power factor can result in optional use of smaller cross-sectional area of line conductors, less thermal insulation and thus smaller investments when constructing transmission and distribution lines. [17, 18]

Different standards define requirements for voltage quality and for permissible voltages in power systems. For example, standard EN 50160 specifies the main characteristics of the electricity supplied by public low, medium and high voltage AC electricity networks [19]. Standard IEC 60038 defines moreover standard voltages in power systems and further permissible voltage drops for different standardized voltage levels [20]. As the voltage needs to be kept at a specific level in the electricity network to fill the power quality requirements set by standards and further specifications, voltage drops across network components must be estimated. This can be calculated with the following equation:

$$\Delta V = \frac{PR+QX}{V} = \frac{PR}{V}\left(1+\frac{QX}{PR}\right), \tag{9}$$

where $X$ is the reactance of the network component. As can be seen, the voltage drop is dependent on both the ratio of reactive power and active power $Q/P$ and the ratio of reactance and resistance $X/R$. To minimize the voltage drop $\Delta V$ the ratio of reactive power to active power should be minimized. The greater the ratio of reactance to resistance is the greater effect is seen in reduction of voltage drop when the ratio $Q/P$ is minimized. [18]

To meet voltage quality requirements and voltage drop limits, conductors with large enough cross-sectional area must be chosen when building new electricity transmission and distribution lines. Correspondingly, the increasing use of electricity and thus a need to transfer more and more power through the same power lines leads to a need for strengthening or renewing of old transmission lines. However, by reducing reactive

power transferred through transmission lines by reactive power compensation it is possible to increase active power transmission capacity of the existing lines without making investments to strengthen or rebuild them. The active power transfer capacity of an existing transmission line can be increased by a factor of $k_c$, as shown in equation 10, if the power factor is improved from $\cos\varphi_a$ to $\cos\varphi_b$.

$$k_c = \left(\frac{\cos\varphi_b}{\cos\varphi_a}\right) \tag{10}$$

Reactive power compensation can reduce the losses along the entire power system and on the other hand make it possible to transfer more active power with the same transmission lines. [17, 18]

Overall, the transmission of reactive power in power systems has numerous disadvantages such as an increase of thermal losses and voltage drops, active power transfer capacity reduction and consequently increased costs of electricity supply. However, reactive power compensation can improve the performance of the whole power system and after all reduce operational costs and costs for investments.

## 3.2 Compensation methods

Reactive power is generated because of reactive loads as noted earlier. In a simple form, depending on whether the load is inductive or capacitive the reactive power component can be compensated by adding either capacitive or inductive component to the grid. This way the original reactive power component will be canceled out as far as the added compensation component is correctly rated. There are several different ways to implement reactive power compensation but overall all compensation methods can be divided into two categories: shunt connected and series connected compensators.

### 3.2.1 Shunt compensation

Usually, a load requires reactive power and draws it from the grid. In other words, a source must provide this reactive power to the grid, which increases line current as noted earlier. The main principle of shunt compensation is to provide this reactive power near the load in which case reactive power is not needed to be transferred from the source through power lines.

Figure 4 illustrates a system consisting of a voltage source, an inductive load and a power line. Moreover, it shows system's phasor diagram in a case without reactive power compensation.

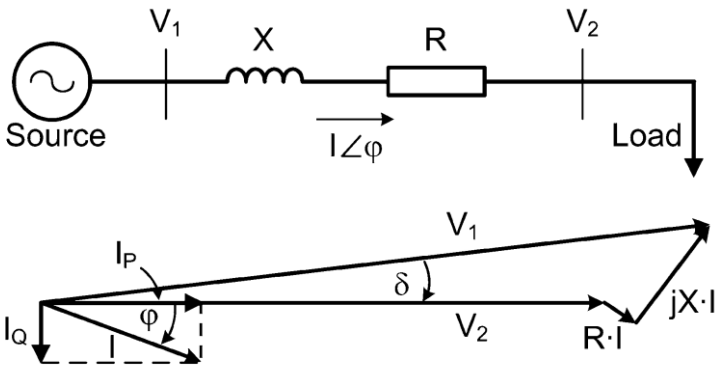


***Figure 4.*** *Power system and its phasor diagram without reactive power compensation [21].*

Current drawn by the load consists of active current $I_P$ and reactive current $I_Q$. In shunt compensation, the reactive part of the current is produced near the load resulting in only active power to be transferred through power lines. Figure 5 shows the same system and its phasor diagram in a case when reactive power compensation is done with a current source.

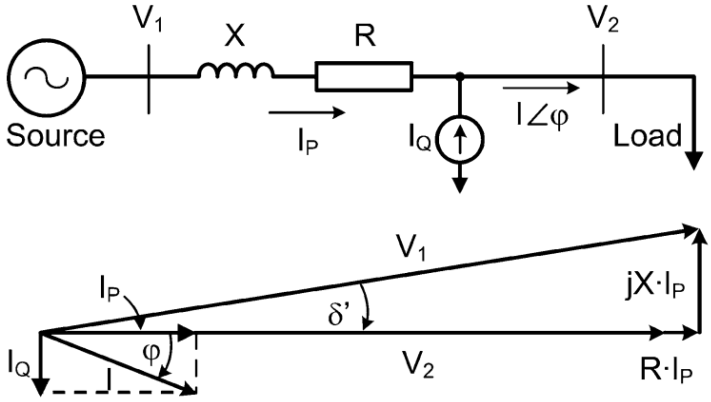


***Figure 5.*** *Shunt compensation with a current source [21].*

As can be seen, the current source produces all the reactive power needed for the load and thus smaller current flows along power lines transferring only active power from the source to the load. [21]

Depending on the case, reactive power compensation by shunt compensators can be done with a capacitor, an inductor, a current source or a voltage source. Traditionally typical loads in electricity network have been inductive as electric motors, transformers and coils are inductive by nature. For this reason, a traditional way to carry out reactive power compensation has been adding capacitor banks to the grid near these inductive loads.

These capacitor banks provide the reactive power needed by inductive loads. More advanced shunt type of reactive power compensation can be done for example with Static Var Compensator (SVC) or Static Synchronous Compensator (STATCOM). [21]

### 3.2.2 Series compensation

Reactive power compensation can also be done with a series compensation system. A common case is to install a series capacitor on a transmission line. Correctly rated capacitor decreases the total reactance of the transmission line resulting in improved performance of the power transfer. The active power transfer over a line can be expressed as follows:

$$P = \frac{V_{n1}V_{n2}}{X_L} sin\,\delta, \tag{11}$$

where $V_{n1}$ is the voltage at the sending end, $V_{n2}$ the voltage at the receiving end and $\delta$ is the phase angle between $V_{n1}$ and $V_{n2}$. In other words, if a capacitor having a reactance $X_C$ is connected in series with the line, the reactance of the line is reduced from $X_L$ to $X_L$-$X_C$. As a result, the active power transfer capacity can be increased. The series capacitor may be located at the sending end, receiving end or at the center of the line. [21]

Series compensation can theoretically be also implemented for example with a voltage source. Figure 6 illustrates the same system as earlier but now the compensation is done with a series type of voltage source installed between a load and the power line.

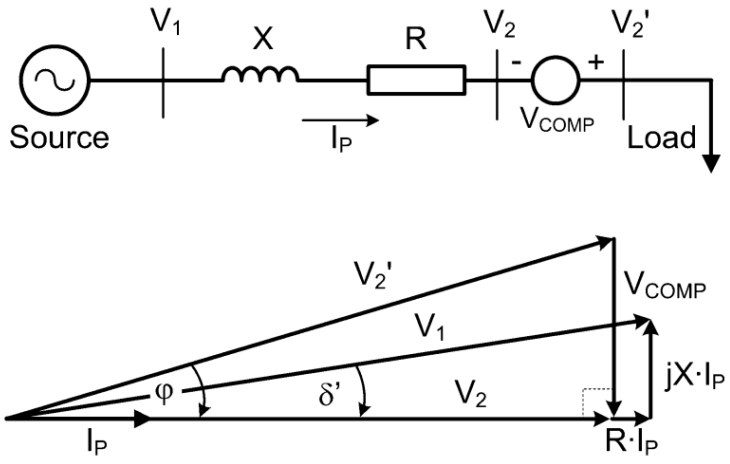


***Figure 6.*** *Series compensation with a voltage source [21].*

As can be seen in Figure 6, when correctly adjusted the voltage source compensator produces its voltage in a way that as a result only active power flows between the source and $V_2$. However, the most common solution for series compensation is to use series capacitors as mentioned earlier. [21]

## 3.3 STATCOM

Static Synchronous Compensator (STATCOM) is a shunt connected reactive power compensation device that is capable of generating and absorbing reactive power. It consists of a controllable, power electronic switches based, voltage-source converter (VSC) which is located behind a coupling reactor. STATCOM can be seen as a solid-state switching converter feeding its output from an energy storage device at its input terminals. STATCOM produces its output based on DC voltage which it modulates according to the reference so that a desired current is achieved with the help of voltage over its coupling reactor. In other words, it provides the wanted reactive power generation and absorption completely through electronic processing of the voltage and current waveforms in a voltage-source converter. STATCOM's one main advantage is that its reactive power compensation capability is not dependent on the grid voltage which thus makes it possible to provide the maximum rated inductive and capacitive current independent of the grid voltage. In other words, by not relying on passive components to produce reactive power, like extensively used conventional Static Var Compensator (SVC) does, STATCOM's undervoltage performance is far greater than SVC's. Moreover, compared to SVC, STATCOM has better dynamic performance, faster response and smaller size (footprint) but with a cost of higher price. [3]

### 3.3.1 Structure and operation principle

STATCOM consists of a controllable voltage-source converter (VSC), a coupling reactor and a coupling or a step-down transformer. The voltage-source converter is a DC to AC converter operated from an energy storage capacitor. STATCOM's basic configuration is presented in Figure 7.

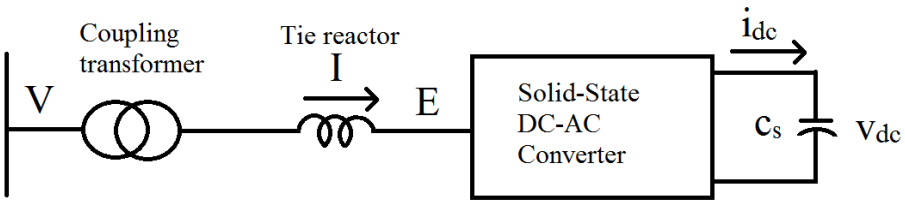


***Figure 7.*** *STATCOM's basic configuration [3].*

To illustrate the basic principle of STATCOM's reactive power generation a simplified equivalent circuit is presented in Figure 8.

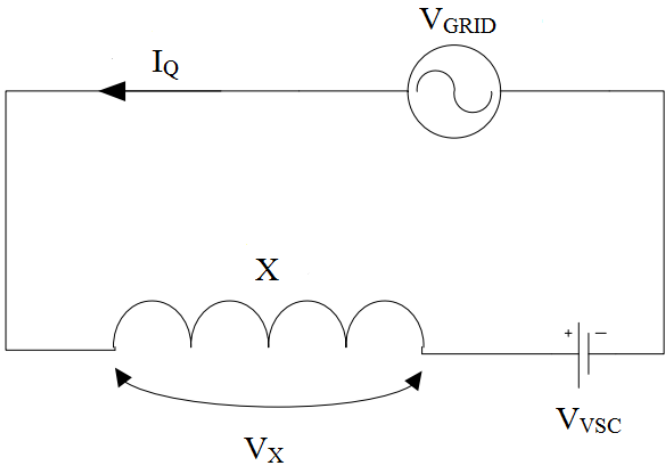


***Figure 8.*** *Simple equivalent circuit of STATCOM.*

The equivalent circuit consists of an ideal voltage source $V_{GRID}$ as grid voltage, which is reduced to the transformer secondary side, Voltage Source Converter $V_{VSC}$ and a reactance $X$ which is a sum of coupling coil and transformer reactances. The reactive power of STATCOM depends on the voltage across the reactance $X$. In other words, reactive current $I_Q$ drawn by STATCOM depends on the voltage magnitude difference between VSC produced $V_{VSC}$ and the grid voltage $V_{GRID}$. If losses are not considered, VSC produces a three-phase voltage $V_{VSC}$ in phase with the three-phase voltage $V_{GRID}$ of the system. Thus, according to the basic circuit theory, reactive current $I_Q$ can be formed with the help of $V_{GRID}$, $X$ and $V_{VSC}$ as presented in equation 12.

$$I_Q = \frac{V_{GRID} - V_{VSC}}{X} \tag{12}$$

As a result, the corresponding reactive power $Q$ drawn from the grid can be expressed as follows:

$$Q = V_{GRID} I_Q = \frac{1 - \frac{V_{VSC}}{V_{GRID}}}{X} {V_{GRID}}^2 \tag{13}$$

On the basis of above equation 13, by controlling the voltage magnitude of the VSC the reactive power flow can also be controlled. If the produced $V_{VSC}$ is greater than $V_{GRID}$ a leading current is produced resulting in capacitive power generated by STATCOM. Respectively, if the grid voltage $V_{GRID}$ is greater, the resulting current lags the grid voltage and thus reactive power is absorbed. In other words, by varying VSC's output voltage magnitude, the reactive power flow between STATCOM and the grid can be controlled. To clarify different operation schemes phasor diagrams are presented in Figure 9.

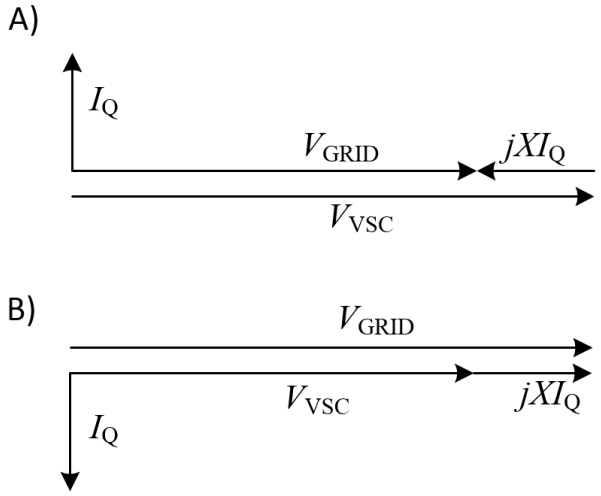


***Figure 9.*** *Phasor diagrams for A) capacitive power and B) inductive power operation schemes.*

Figure 9A) illustrates the capacitive power operation scheme and respectively Figure 9B) presents the inductive power operation scheme. If the produced $V_{VSC}$ magnitude equals $V_{GRID}$, the voltage across reactance $X$ is zero and thus STATCOM operates at its zero-operation point which means no reactive power flows between the grid and STATCOM. [3]

In an ideal case, STATCOM would produce sinusoidal output voltage, draw sinusoidal reactive current and moreover the DC capacitor average current would equal zero. In practice, due to switching losses and other internal losses the energy stored in the DC capacitor would discharge if the losses were not compensated. The compensation can be done by making the produced voltage lag the grid voltage by a small angle which results in active power being supplied from the grid to cover the internal losses in VSC. This method is based on equation 11. Hence, the DC capacitor voltage can be kept at a desired level. Moreover, as the produced voltage is never a perfect sinusoid, harmonics are generated to the grid. [3]

### 3.3.2 Switching devices and converter topologies

There are various controllable solid-state switches that can be used in VSCs but only few are suitable for high power applications. Each switching device has different operating characteristics as well as strengths and weaknesses in respect to rated power, switching frequency, switching losses etc. A Gate-Turn-Off thyristor (GTO) and an Insulated Gate Bipolar Transistor (IGBT) are the most commonly used switches in high power applications. GTO is a mature technology with higher power ratings whereas IGBT is newer technology in power electronics with higher switching frequency and speed as well as lower losses. [22]

The simplest converter topologies capable of producing AC output from DC input are two-level and three-level converters where the number of levels refers to possible output voltage levels. For example, a two-level converter can only produce positive and negative voltages i.e. simple square-wave whereas a three-level converter can produce positive, negative and zero outputs. Naturally, the produced voltage waveform with two and three-level converters is not of the same shape with an ideal sinewave which means a great number of harmonics being created. In order to reduce the harmonic content in the produced voltage, the simple three-level converter can be extended to a multi-level converter thus enabling a production of better sinusoidal waveforms. [22] In other words, with multi-level converters the switches are controlled in a way to produce a staircase voltage waveform that approximates a sinusoid. However, the circuit and control complexity increases significantly with the increasing number of voltage levels.

The switching is usually done either according to fundamental switching method or with Pulse Width Modulation (PWM) method. In fundamental switching method switching is done once in a fundamental cycle which results in a great number of harmonics occurring in the output voltage. On the other hand, with PWM method the switching can be done multiple times in one cycle which thus reduces harmonics created similar with the multi-level converter topology. However, as switching times increase with PWM method, naturally also more switching losses are generated. [22]

### 3.3.3 Studied STATCOM

In this thesis, Modular Multilevel Converter (MMC) based STATCOM is studied. MMC is a type of a multi-level converter that consists of multiple submodules connected in series. Each submodule consists of four IGBT switches that have antiparallel-connected diodes. In other words, each submodule has so called full-bridge topology that can produce three output voltage levels thus making one submodule act as a three-level converter topology. The total voltage of one phase is formed as a sum of individual submodule voltages consequently making it possible to produce $2n+1$ voltage levels, where $n$ corresponds to the number of submodules in series.

The series-connected submodule structure in one phase is called a branch. In this thesis, a three-phase converter topology is achieved by connecting the three branches in delta (delta-connected STATCOM). Moreover, a wye-delta connected step-down transformer is used to connect STATCOM to the grid. These delta connections affect voltage and current positive and negative sequence components differently which needs to be considered when implementing the active filter feature.

# 4. HARMONICS DETECTION METHODS AND GRID SYNCHRONIZATION

Detection methods used for harmonics compensation can be generally categorized into frequency domain methods and time domain methods. In this chapter, two time domain based methods, a Second Order Generalized Integrator based method and a synchronous reference frame based method, are studied. The basic theory and operation principles of these two methods are presented and their suitabilities to be used in the studied STATCOM system are considered.

## 4.1 Second Order Generalized Integrator

A concept for a voltage positive sequence component detection by Second Order Generalized Integrator (SOGI) was originally presented by P. Rodriguez in [23]. This method is since further developed to suit for harmonics detection and compensation as a frequency adaptive filter. SOGI has similarities for example with a Proportional-Resonant -controller (PR-controller) structure where generalized integrator part is also introduced. Figure 10 presents the structure of the SOGI.

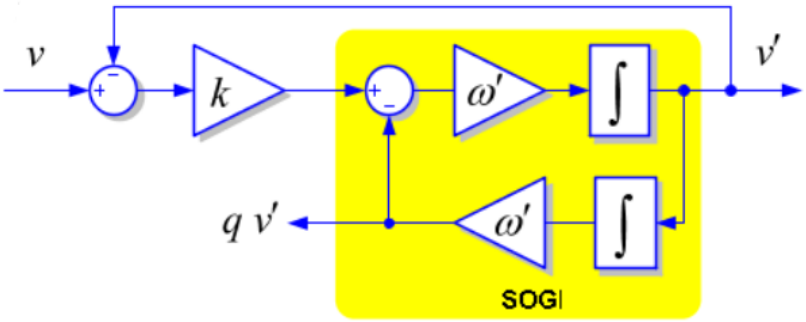


***Figure 10.*** *Structure of a single SOGI [23].*

In Figure 10, $v$ is the instantaneous input voltage signal, $v'$ and $qv'$ are two inquadrature output signals and $k$ and $\omega'$ are referred as SOGI's gain and resonance frequency, respectively. The output signal $v'$ is in phase with the input signal $v$ having also the same magnitude whereas the $qv'$ is in 90 degrees phase shift lagging thus both $v$ and $v'$. Transfer functions from input signal $v$ to output signals $v'$ and $qv'$ are presented in equations 14 and 15.

$$D(s) = \frac{v\prime}{v} = \frac{k\omega' s}{s^2 + k\omega' s + \omega'^2} \tag{14}$$

$$Q(s) = \frac{qv\prime}{v} = \frac{k\omega'^2}{s^2 + k\omega' s + \omega'^2} \tag{15}$$

In Figure 11, bode diagrams for $D(s)$ and $Q(s)$ are presented when SOGI gain $k$ is 1.41 and resonance frequency $\omega'$ is set to 314 rad/s.

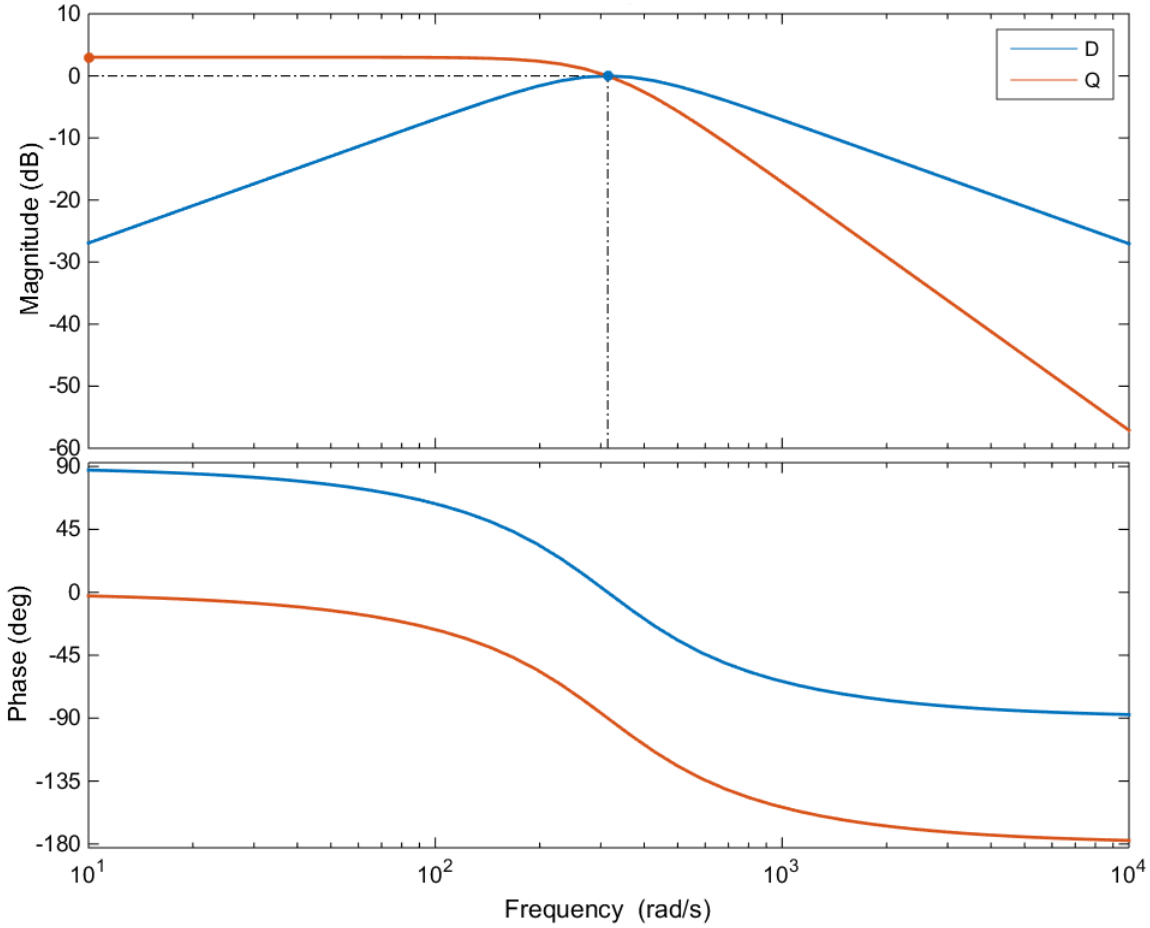


***Figure 11.*** *Bode diagrams for D(s) and Q(s).*

As can be noticed in Figure 11, SOGI works as a bandpass filter introducing zero dB gain and zero phase shift at SOGI's resonance frequency $\omega'$. Equations 16–19 present gain and phase shift calculation for $D(s)$ and $Q(s)$.

$$|D| = \frac{k\omega'\omega}{\sqrt{(k\omega'\omega)^2+(\omega'^2-\omega^2)^2}} \tag{16}$$

$$\angle D = tan^{-1}\left(\frac{\omega'^2-\omega^2}{k\omega'\omega}\right) \tag{17}$$

$$|Q| = \frac{\omega'}{\omega}|D| \tag{18}$$

$$\angle Q = \angle D - \frac{\pi}{2} \tag{19}$$

In above equations, $\omega$ represents the input signal's frequency. It can be noticed based on above equations, as well as from the bode diagrams presented in Figure 11, that $qv'$ is always lagging 90 degrees behind $v'$ independent from resonance frequency $\omega'$ and input signal $v$. [23]

Unlike it is stated in [24], the bandwidth of $D(s)$ isn't set only by $k$ completely independent of the resonance frequency $\omega'$. The bandwidth is actually the product of $k$ and $\omega'$. However, when the resonance frequency is set then the dynamics of SOGI can be set exclusively by $k$. Thus, increasing $k$ corresponds to faster response resulting in also lower selectivity. On the other hand, by decreasing $k$, a better selectivity can be achieved with the cost of slower response. For the fundamental frequency SOGI, a critically-damped response can be obtained with $k$ equal to $\sqrt{2}$ [23].

When input signal frequency $\omega$ and SOGI's resonant frequency $\omega'$ are exactly the same, the output signal's amplitude follows the input signal's amplitude. If this is violated, as is the case often in real life systems, SOGI may lose its tracking accuracy resulting in incorrect signal detection. This can also be noticed in equations 16–19. In other words, a constant resonant frequency can only be used when the input signal frequency is known and has no variation. To make SOGI's resonant frequency adaptive for input signal frequency variation a Frequency Locked Loop (FLL) is introduced. Figure 12 presents the structure of SOGI with FLL.

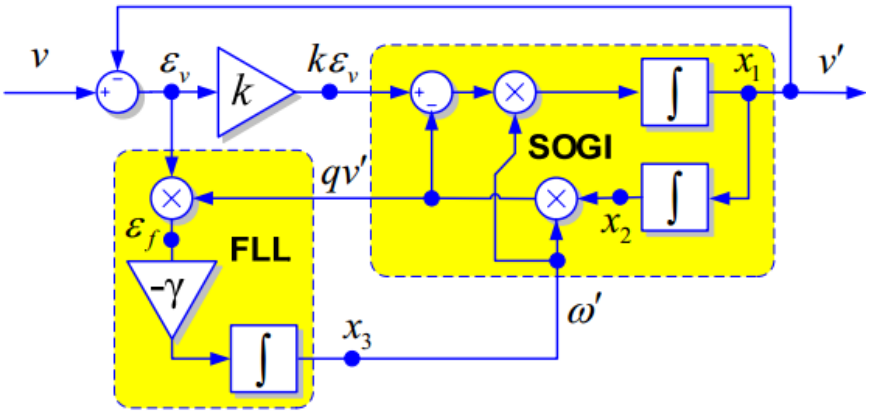


***Figure 12.*** *Structure of FLL with SOGI [24].*

As can be seen in Figure 12, input signals for FLL are SOGI's output signal $qv'$ and error signal $\varepsilon_v$. $\gamma$ in the FLL block is called FLL gain and $\varepsilon_f$ respectively the frequency error variable. The transfer function for signal $\varepsilon_v$ is presented in 20.

$$E(s) = \frac{\varepsilon_v}{v} = \frac{s^2+\omega'^2}{s^2+k\omega' s+\omega'^2} \tag{20}$$

Signals $qv'$ and $\varepsilon_v$ are in phase with each other always when SOGI's resonant frequency i.e. the output signal of FLL is greater than the input signal frequency. However, when the frequency of the input signal is greater than the resonant frequency of SOGI, signals $qv'$ and $\varepsilon_v$ have 180 degrees phase shift. Bode diagrams in Figure 13 justify this.

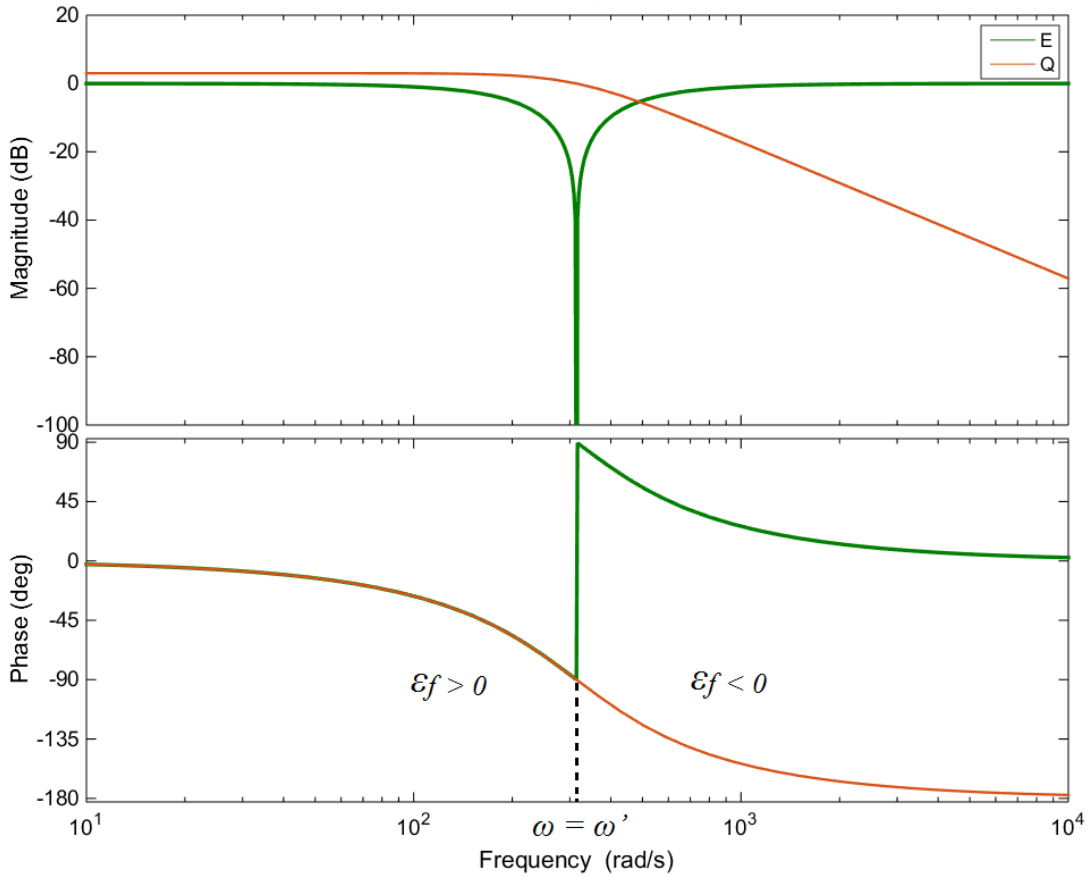


***Figure 13.*** *Bode diagrams for FLL E(s) and Q(s).*

It can be detected by the product of these two signals whether the resonant frequency of SOGI needs to be increased or decreased to meet the input signal frequency. The FLL uses integrator controller with a negative gain $\gamma$ to find the true input signal frequency. In other words, $\varepsilon_f$, the product of $qv'$ and $\varepsilon_v$, is negative when the input frequency is greater than SOGI's resonant frequency thus increasing the value of FLL's output signal. Respectively, the product of $qv'$ and $\varepsilon_v$ is positive when the input frequency is lower than SOGI's resonant frequency and decreases therefore the value of FLL's output signal $\omega'$. Hence with FLL, SOGI automatically tunes its resonant frequency to its input signal's frequency. [24]

The FLL has nonlinear dynamics with changing grid voltage. However, the FLL can be normalized and thus made as a linearized system independent of grid variables and the SOGI gain $k$ as derived in [24]. Figure 14 shows the FLL block with the gain normalization.

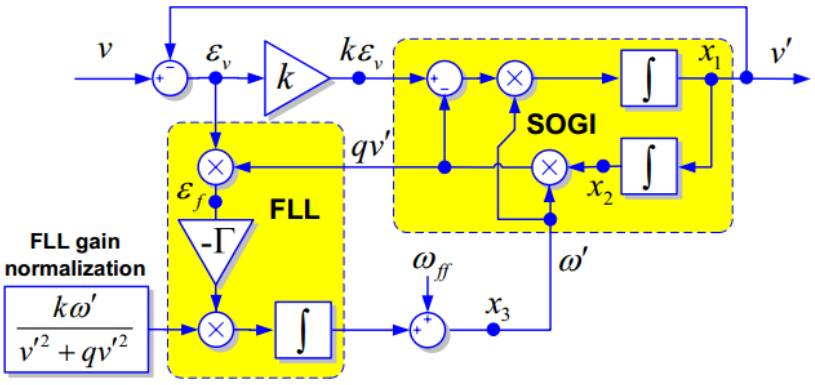


***Figure 14.*** *Structure of normalized FLL with SOGI [24].*

The new FLL uses also a feedforward term $\omega_{ff}$ to speed up the frequency detection as can be seen in Figure 14.

### 4.1.1 DSOGI

For three-phase systems SOGI-FLL can be upgraded to Double Second Order Generalized Integrator (DSOGI) consisting of two individual SOGIs and a single FLL as presented in [25]. In this case, a three-phase input vector $\boldsymbol{v}_{abc}$ is transformed to a voltage vector $\boldsymbol{v}_{\alpha\beta}$ in αβ stationary reference frame by using the Clarke transformation. The Clarke transformation is presented in equations 21 and 22.

$$\boldsymbol{v}_{\alpha\beta} = [\boldsymbol{T}_{\alpha\beta}]\boldsymbol{v}_{abc} \tag{21}$$

$$[\boldsymbol{T}_{\alpha\beta}] = \frac{2}{3}\begin{bmatrix} 1 & -\frac{1}{2} & -\frac{1}{2} \\ 0 & \frac{\sqrt{3}}{2} & -\frac{\sqrt{3}}{2} \end{bmatrix} \tag{22}$$

The inverse Clarke transformation can be derived based on equation 22. Amplitude-invariant Clarke transformation is used, unlike in [25] where power-invariant transformation is used, in order to preserve original signal's amplitude unchanged. In three-phase systems, the analysis of especially unbalanced grid conditions can be simplified by using so called symmetrical components. Symmetrical components consist of positive, negative and zero sequence components. Positive sequence components are equal in magnitude and have phase shifts of 120 degrees in each phase. The phase sequence is the same as with the original phase quantities (A-B-C). Negative sequence components are also equal in magnitude and have the same 120 degrees phase shifts but in a reverse phase sequence (A-C-B). Zero sequence components, in turn, are equal in magnitude and in phase. [26] Equation 22 represents the relation between phase voltages and symmetrical components.

$$\begin{bmatrix} V_a \\ V_b \\ V_c \end{bmatrix} = \begin{bmatrix} 1 & 1 & 1 \\ a^2 & a & 1 \\ a & a^2 & 1 \end{bmatrix} \begin{bmatrix} V_a^+ \\ V_a^- \\ V_a^0 \end{bmatrix} \tag{23}$$

In equation 23, $V_a$, $V_b$ and $V_c$ are voltage phasors of each phase, $a$ represents a 120 degrees phase shift and superscripts +, – and 0 represent positive, negative and zero sequence components. These symmetrical components replace the normal phase quantities in the analysis of three-phase systems. As a consequence, a division to positive and negative sequence αβ components in stationary reference frame can be done with the help of SOGI's inquadrature output signals as shown in equations 24 and 25.

$$\boldsymbol{v}_{\alpha\beta}{}^{+} = [\boldsymbol{T}_{\alpha\beta}]v_{abc}{}^{+} = [\boldsymbol{T}_{\alpha\beta}][\boldsymbol{T}_{+}]\boldsymbol{v}_{abc} = [\boldsymbol{T}_{\alpha\beta}][\boldsymbol{T}_{+}][\boldsymbol{T}_{\alpha\beta}]^{T}\boldsymbol{v}_{\alpha\beta} = \frac{1}{2}\begin{bmatrix}1 & -q\\ q & 1\end{bmatrix}\boldsymbol{v}_{\alpha\beta} \quad (24)$$

$$\boldsymbol{v}_{\alpha\beta}{}^{-} = [\boldsymbol{T}_{\alpha\beta}]\boldsymbol{v}_{abc}{}^{-} = [\boldsymbol{T}_{\alpha\beta}][\boldsymbol{T}_{-}]\boldsymbol{v}_{abc} = [\boldsymbol{T}_{\alpha\beta}][\boldsymbol{T}_{-}][\boldsymbol{T}_{\alpha\beta}]^{T}\boldsymbol{v}_{\alpha\beta} = \frac{1}{2}\begin{bmatrix}1 & q\\ -q & 1\end{bmatrix}\boldsymbol{v}_{\alpha\beta} \quad (25)$$

In above equations, $q$ denotes $e^{\frac{-j\pi}{2}}$ i.e. 90 degrees phase shift. Based on equations 24 and 25 two SOGIs are implemented, one for each $v_\alpha$ and $v_\beta$ component. The structure of DSOGI-FLL is presented in Figure 15.

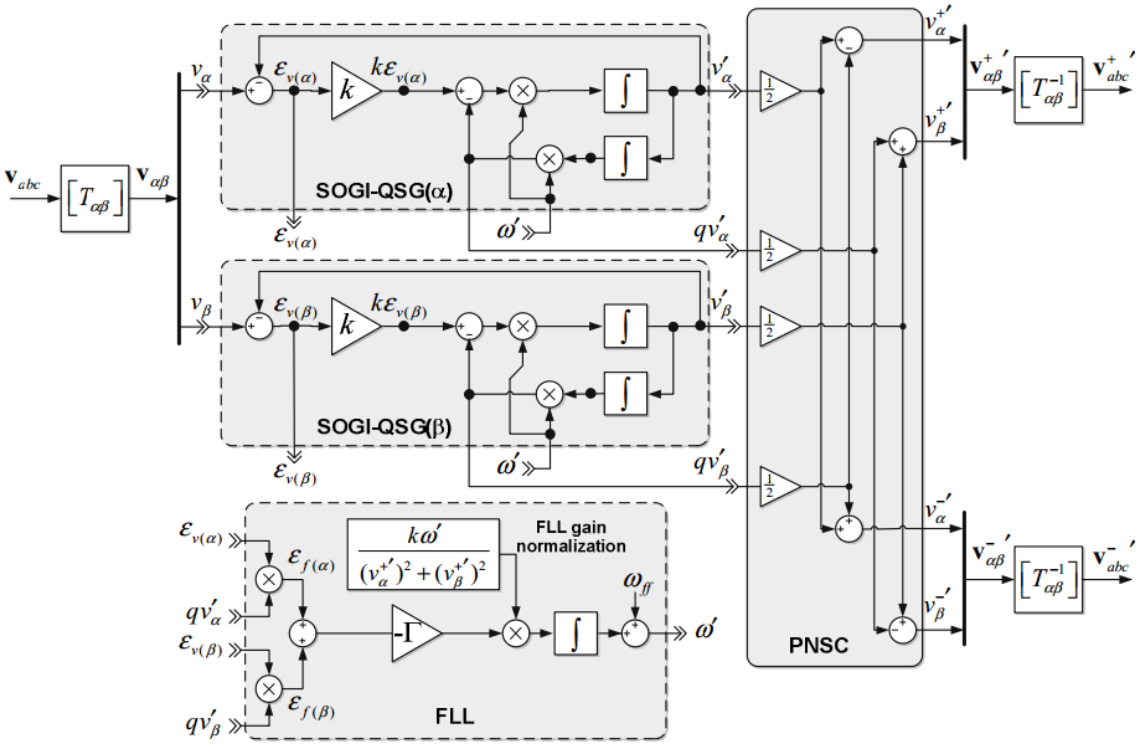


***Figure 15.*** *DSOGI-FLL with PNSC for positive and negative sequence extraction [25].*

DSOGI uses only one FLL that adapts the resonant frequency of both SOGIs to input signal frequency as can be seen in Figure 15. PNSC, in turn, is the Positive Negative Sequence Calculator based on equations 24 and 25. Finally, after positive and negative sequence components for $v_\alpha$ and $v_\beta$ are calculated, the inverse Clarke transformation can be used to solve instantaneous positive and negative sequence components of the phase voltages. [25]

### 4.1.2 MSOGI

Previously presented structures work with detecting the fundamental component of the input signal. However, to detect multiple harmonics a structure for Multiple Second Order Generalized Integrator (MSOGI) or more precisely Multiple Double Second Order Generalized Integrator (MDSOGI) is introduced. MSOGI uses individual SOGIs tuned at different frequencies to extract the fundamental component and selected harmonics from the input signal. The structure of MSOGI with FLL is presented in Figure 16.

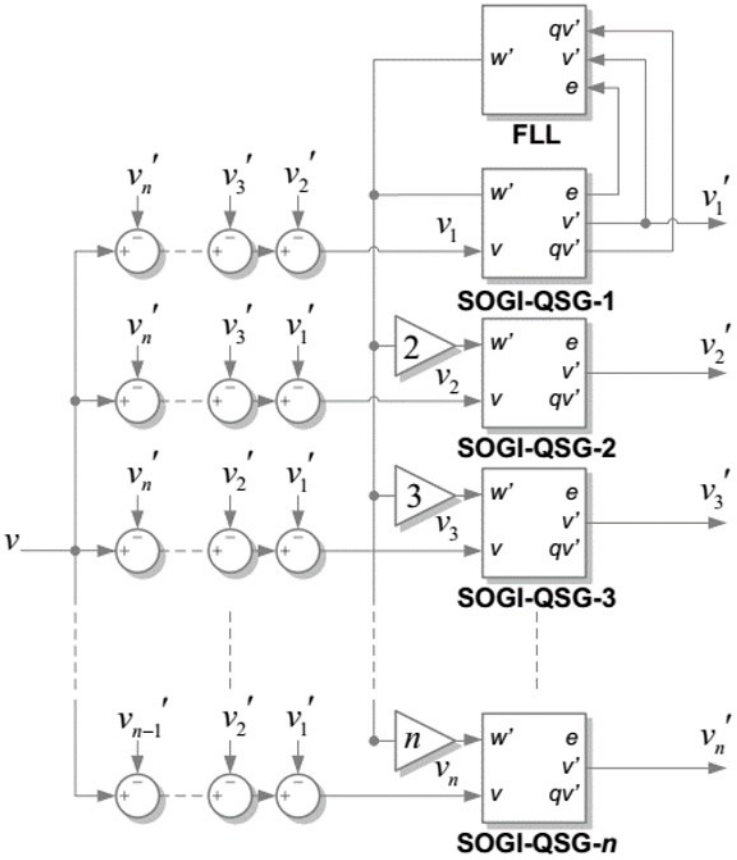


***Figure 16.*** *Multiple SOGIs working in parallel and a cross-feedback network [24].*

As can be seen in Figure 16, individual SOGIs tuned at different frequencies work in parallel in order to extract the fundamental component and selected harmonics from the input signal. The FLL uses only the SOGI block of the fundamental component to detect the fundamental frequency which is then multiplied by a harmonic order and forwarded for each SOGI with the corresponding harmonic order. As can also be seen in Figure 16, a cross-feedback network can be used to radically enhance the accuracy of the MSOGI system. This is necessary especially when SOGIs are tuned at frequencies close to each other as is the case with harmonics detection. In other words, each SOGI's input signal is comprised by subtracting all the outputs of other SOGIs from the original input signal. Thus, in an ideal case each SOGI's input should in the end only contain the particular harmonic component or the fundamental one. [25]

Each SOGI can be replaced with DSOGI to obtain positive-negative sequence tracking in three-phase systems for selected harmonics. For this use, a Positive Negative Sequence Calculator can again be used similar with the structure in Figure 15. In three-phase systems, Clarke transformation can be implemented before the actual cross-feedback network to reduce the number of operations. In this case, only two components, α and β, need to be brought back to the cross-feedback network in comparison to three components if done with three-phase signals. [25]

As mentioned, the bandwidth of SOGI is the product of its gain *k* and resonance frequency *ω'*. Furthermore, a critically-damped response for the fundamental SOGI can be achieved with *k* equal to √2. Thus, to achieve a critically-damped response for the rest of the SOGIs, the gain of each SOGI is set by dividing the gain of the fundamental SOGI with the harmonic order *h* of the SOGI in question. In this thesis, MSOGI is further studied i.e. used in simulations.

### 4.1.3 Phase shift due to delta-connections and grid impedance

In this thesis, in general terms, harmonics compensation is done by measuring the phase voltages at the point of common coupling (PCC), detecting harmonics with the help of e.g. MSOGI and by creating a reference current that produces the wanted VSC voltage and thus the wanted compensation current. As mentioned in chapter 3.3.3 the system studied is a delta-connected STATCOM behind a star-delta connected stepdown transformer. Positive and negative sequence voltages and currents undergo a phase shift when passing through these delta connections. In Figure 17, a star-delta connected transformer is considered with winding polarities as shown in the figure.

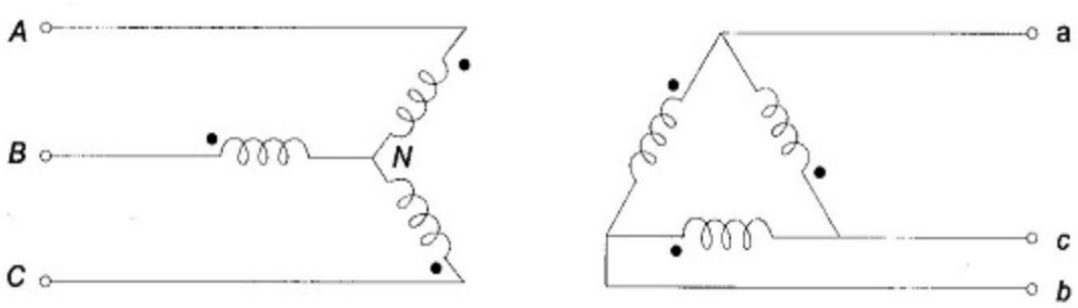


***Figure 17.*** *A star-delta connected transformer [27].*

Based on Figure 17, a phasor diagram for positive sequence voltages at transformer primary and secondary sides can be drawn. Phasor diagram is presented in Figure 18.

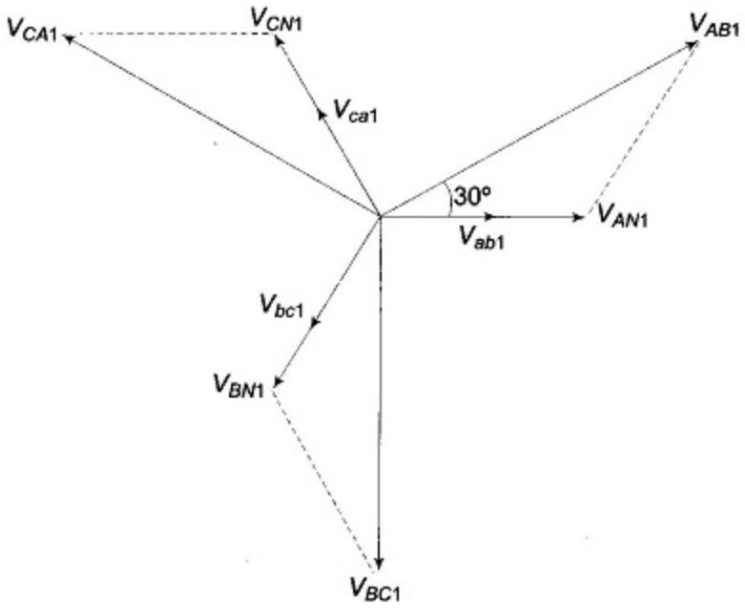


***Figure 18.*** *Positive sequence voltages on Yd1 transformer [27].*

The notation is done so that $V_{AB1}$, $V_{BC1}$, $V_{CA1}$ are the line-to-line voltages and $V_{AN1}$, $V_{BN1}$, $V_{CN1}$ are the phase voltages on the primary star side. Respectively, $V_{ab1}$, $V_{bc1}$ and $V_{ca1}$ denote the corresponding line-to-line voltages on the secondary delta side. As can be seen, the positive sequence line voltages on star side lead the corresponding delta side quantities by 30 degrees. The same phase shifts are also valid for currents. The transformer in Figure 17 is thus Yd1 type of transformer.

If negative sequence voltages are considered, the phase shift reverse. A phasor diagram is presented in Figure 19 to illustrate the phase shifts in case of negative sequence quantities.

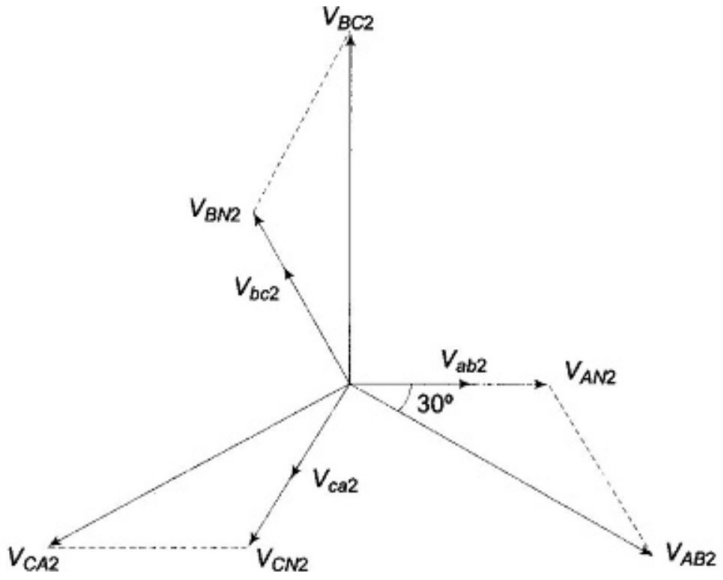


***Figure 19.*** *Negative sequence voltages on Yd1 transformer [27].*

As can be seen in Figure 19, for negative sequence voltages the phase shift is reverse which means that the star side quantities lag delta side quantities by 30 degrees.

In this thesis, Yd11 type of transformer is used which means that for positive sequence quantities delta side leads by 30 degrees and respectively for negative sequence quantities star side leads by 30 degrees. [26] Moreover, due to delta-connected STATCOM branches additional 30 degrees phase shifts occur when the produced compensation current passes through the STATCOM delta-connection. The positive sequence quantities in STATCOM's delta-connection lead by 30 degrees whereas the negative sequence quantities in delta-connection lag by 30 degrees in respect to corresponding quantities outside the delta-connection. In other words, positive and negative sequence quantities undergo altogether 60 degrees phase shifts (to reverse directions) due to Yd11 type of transformer and the delta-connected STATCOM branches.

In addition to delta-connections' phase shifts, to be able to implement harmonics compensation accurately, the grid impedance should also be known. The grid impedance causes a phase shift between the injected harmonic compensation current and the resulting voltage drop which thus needs to be taken into account similar with the phase shifts caused by the delta-connections. The resulting voltage drop is presented in equation 26.

$$\Delta v^h = z^h_{GRID} i^h \tag{26}$$

In other words, the grid impedance $z^{\mathrm{h}}_{\mathrm{GRID}}$ at a harmonic frequency $h$ produces a voltage drop $\Delta v^{\mathrm{h}}$ due to a harmonic current $i^{\mathrm{h}}$ flowing through it. Typically, the grid impedance can be assumed to be inductive. In that case, the produced voltage drop $\Delta v^{\mathrm{h}}$ leads the harmonic current $i^{\mathrm{h}}$ by 90 degrees in both positive and negative sequence cases. On the other hand, if the grid impedance is purely capacitive, the resulting voltage drop would lag 90 degrees behind the harmonic current. However, in practise the grid impedance is never purely inductive nor capacitive but includes also a resistive part. In other words, the phase shift can therefore vary completely between -90 degrees and 90 degrees. In this thesis, a highly inductive (inductive-resistive) grid impedance is assumed. The phase shift due to the grid impedance is approximated to be 90 degrees for both positive and negative sequence components which is justified as the grid reactance is much larger compared to the grid resistance. Moreover, the grid reactance increases as a function of frequency and thus makes the grid impedance to appear more and more inductive as the frequency increases.

As stated, the positive sequence current in STATCOM delta branch leads the current at PCC by 60 degrees. The corresponding voltage drop, however, leads the PCC current by 90 degrees and thus in the control system the reference vector should be lagged by 30 degrees to neutralize the phase shift effects. Respectively, for the negative sequence, the current in STATCOM delta branch lags the corresponding PCC current by 60 degrees. On the other hand, the voltage drop leads the PCC current by 90 degrees and thus in the

control system the reference vector should be lagged by 150 degrees to compensate the phase shift effects.

Altogether, the phase shifts needed to compensate the effects of the star-delta connected transformer, delta connected STATCOM as well as the grid impedance angle must be implemented for positive and negative sequence components separately. In MSOGI this can be done with a rotation matrix in the αβ-frame as αβ-components form a complex plane. Individual rotation matrixes can be used for positive and negative sequence components to enable separate positive-negative sequence phase control. The rotation matrix is presented in the following equations 27 and 28.

$$\boldsymbol{R}(\theta) = \begin{bmatrix} cos\,\theta & -sin\,\theta \\ sin\,\theta & cos\,\theta \end{bmatrix} \tag{27}$$

$$\boldsymbol{v}_{\alpha\beta,rotated} = \boldsymbol{R}\boldsymbol{v}_{\alpha\beta} \tag{28}$$

The rotation matrix rotates the vector $\boldsymbol{v}_{\alpha\beta}$ counter-clockwise by an angle $\theta$ introduced in the rotation matrix resulting in a rotated voltage vector $\boldsymbol{v}_{\alpha\beta,\text{rotated}}$. If rotation to a clockwise direction is wanted then a negative angle must be presented.

## 4.2 Synchronous reference frame

The detection and control of the fundamental voltage component can be done with the help of synchronous reference frame (SRF). The main idea is to transform the rotating three-phase components from the natural abc reference frame to DC values in the rotating dq reference frame. This can be done by first using the Clarke transformation, as was done also with SOGI, to transform the three-phase components to two inquadrature components in the stationary reference frame and then applying the Park transformation. The Park transformation makes the coordinate system to rotate to the same direction with the same angular speed as αβ components. As a result, αβ components are transformed to a voltage vector $\boldsymbol{v}_{\text{dq}}$ i.e. d and q components, which are DC values, in the synchronous reference frame. [28] The Park transformation is presented in equations 29 and 30.

$$\boldsymbol{v}_{dq} = \begin{bmatrix} v_d \\ v_q \end{bmatrix} = [\boldsymbol{T}_{dq}]\boldsymbol{v}_{\alpha\beta} \tag{29}$$

$$[\boldsymbol{T}_{dq}] = \begin{bmatrix} cos\,\theta_{sync} & sin\,\theta_{sync} \\ -sin\,\theta_{sync} & cos\,\theta_{sync} \end{bmatrix} \tag{30}$$

In equation 30, $\theta_{\text{sync}}$ is a so-called angular position which defines the rotation angle. As can be noticed, the Park transformation is basically a rotation matrix which just rotates the αβ components all the time to their reverse direction thus resulting in non-rotating d and q components. The inverse Park transformation can be derived based on equation 30.

The angular position needed in the Park transformation is obtained conventionally by using a Phase-Locked Loop (PLL) method. PLL gives the angle of the voltage component

in reference to d component by controlling the voltage q component to zero. [28] The structure of the PLL block is presented in Figure 20

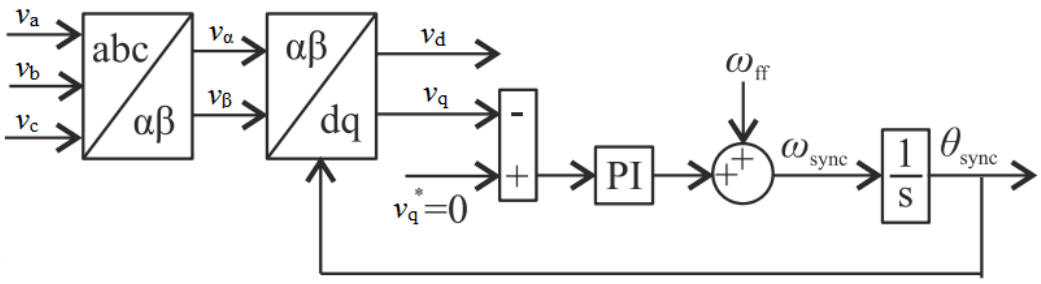


***Figure 20.*** *Structure of the Phase-Locked Loop. Figure adapted from figure in [28].*

As can be seen in Figure 20, a PI-controller is used to control the voltage q component to zero. Moreover, a feedforward term $\omega_{ff}$ is used to speed up the frequency tracking and finally the angular position $\theta_{sync}$ is obtained after integration of $\omega_{sync}$.

### 4.2.1 Decoupled Double Synchronous Reference Frame

For unbalanced grid conditions SRF-PLL can be upgraded to Decoupled Double Synchronous Reference Frame PLL (DDSRF-PLL). It uses two different synchronous reference frames, one rotating to positive and the other rotating to negative direction. The positive sequence of the fundamental component can thus be detected with the reference frame rotating to positive direction while the negative sequence component can be detected with the reference frame rotating to the inverse direction, respectively. [28]

Under unbalanced grid conditions the αβ components can be expressed as follows:

$$\boldsymbol{v}_{\alpha\beta} = \begin{bmatrix} v_\alpha \\ v_\beta \end{bmatrix} = U^+ \begin{bmatrix} cos(\omega t + \varphi^+) \\ sin(\omega t + \varphi^+) \end{bmatrix} + U^- \begin{bmatrix} cos(-\omega t + \varphi^-) \\ sin(-\omega t + \varphi^-) \end{bmatrix}, \tag{31}$$

where $\omega t$ represents the angle of the fundamental frequency positive sequence component i.e. $\theta_{sync}$. $U$ and $\varphi$ in turn are the magnitude and the initial angle of the voltage vector. Superscripts + and – denote the positive and negative sequence references, respectively. [28] By using the above equation, the positive and negative sequence components can also be expressed in the synchronous reference frame as follows:

$$\boldsymbol{v}_{dq}^+ = \begin{bmatrix} v_d^+ \\ v_q^+ \end{bmatrix} = [\boldsymbol{T}_{dq}^+] \begin{bmatrix} v_\alpha \\ v_\beta \end{bmatrix} = \begin{bmatrix} cos(\omega t) & sin(\omega t) \\ -sin(\omega t) & cos(\omega t) \end{bmatrix} \begin{bmatrix} v_\alpha \\ v_\beta \end{bmatrix} \tag{32}$$

$$= U^+ \begin{bmatrix} \cos(\varphi^+) \\ \sin(\varphi^+) \end{bmatrix} + U^- \cos(\varphi^-) \begin{bmatrix} \cos(2\omega t) \\ -\sin(2\omega t) \end{bmatrix} + U^- \sin(\varphi^-) \begin{bmatrix} \sin(2\omega t) \\ \cos(2\omega t) \end{bmatrix}$$

$$\boldsymbol{v}_{dq}^{-} = \begin{bmatrix} v_d^- \\ v_q^- \end{bmatrix} = [\boldsymbol{T}_{dq}^{-}] \begin{bmatrix} v_\alpha \\ v_\beta \end{bmatrix} = \begin{bmatrix} cos(\omega t) & -sin(\omega t) \\ sin(\omega t) & cos(\omega t) \end{bmatrix} \begin{bmatrix} v_\alpha \\ v_\beta \end{bmatrix} \quad (33)$$

$$= U^- \begin{bmatrix} \cos(\varphi^-) \\ \sin(\varphi^-) \end{bmatrix} + U^+ \cos(\varphi^+) \begin{bmatrix} \cos(2\omega t) \\ \sin(2\omega t) \end{bmatrix} + U^+ \sin(\varphi^+) \begin{bmatrix} -\sin(2\omega t) \\ \cos(2\omega t) \end{bmatrix}$$

As can be noticed, under unbalanced grid conditions the positive and negative sequence components in the synchronous reference frame consist of DC (Direct Current) and AC (Alternating Current) components. The AC component occurring in the positive sequence reference frame is due to a negative sequence component and the AC component taking place in the negative sequence reference frame respectively is due to a positive sequence component. In other words, under balanced grid conditions when the negative sequence component can be assumed to be zero, the positive sequence component contains only the DC component. A decoupling network is presented to cancel out these AC components thus making it possible to represent the positive and negative sequence components as pure DC components. The DC values can consequently be calculated as shown in equations 34 and 35.

$$U^+ \begin{bmatrix} cos(\varphi^+) \\ sin(\varphi^+) \end{bmatrix} = \begin{bmatrix} U_d^+ \\ U_q^+ \end{bmatrix} = \begin{bmatrix} v_d^+ \\ v_q^+ \end{bmatrix} - U^- cos(\varphi^-) \begin{bmatrix} cos(2\omega t) \\ -sin(2\omega t) \end{bmatrix} - U^- sin(\varphi^-) \begin{bmatrix} sin(2\omega t) \\ cos(2\omega t) \end{bmatrix} \quad (34)$$

$$U^- \begin{bmatrix} cos(\varphi^-) \\ sin(\varphi^-) \end{bmatrix} = \begin{bmatrix} U_d^- \\ U_q^- \end{bmatrix} = \begin{bmatrix} v_d^- \\ v_q^- \end{bmatrix} - U^+ cos(\varphi^+) \begin{bmatrix} cos(2\omega t) \\ sin(2\omega t) \end{bmatrix} - U^+ sin(\varphi^+) \begin{bmatrix} -sin(2\omega t) \\ cos(2\omega t) \end{bmatrix} \quad (35)$$

$U_\mathrm{d}$ and $U_\mathrm{q}$ represent the d and q component pure DC values after the AC components have been cancelled out by the decoupling network. Superscripts + and – represent again positive and negative sequence components, respectively. With the help of above presented decoupling network it is possible to present the desired sequence components as pure DC values. [28]

The phase angle $\omega t$ needed for DDSRF is obtained with PLL similar with the way used in SRF-PLL. The synchronization is done to positive sequence d component. In DDSRF-PLL the PLL block controls the positive sequence q component to zero and thus makes it also possible to represent the positive sequence voltage magnitude using only $U_\mathrm{d}^+$. [28] The structure of the DDSRF-PLL block is presented in Figure 21.

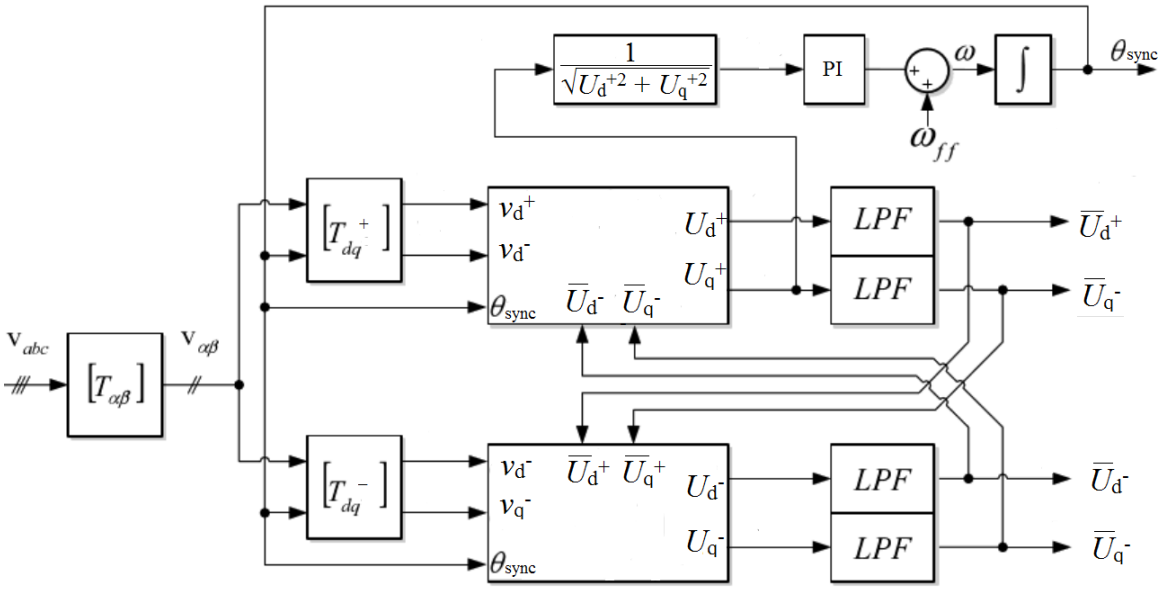


***Figure 21.*** *Structure of DDSRF-PLL. Figure adapted from figure in [28].*

As can be seen in Figure 21, the positive sequence q component used for the synchronization in PLL is normalized to the positive sequence voltage component in order to make the PLL gain remain constant independent of the network voltage magnitude. Moreover, simple low-pass filters are used to extract the DC components for the outputs and for the decoupling networks. [28] A transfer function for the simple low-pass filter is presented in equation 36:

$$LPF(s) = \frac{\omega_f}{s+\omega_f}, \tag{36}$$

where $\omega_f$ is the cut-off frequency. The overbars, used in Figure 21, are to clarify that the corresponding values are really DC values. After a transition period, also the values before low-pass filters are DC values if harmonics are ignored.

In ideal conditions when the grid doesn't consist of any harmonics, the d and q components are pure DC values after the decoupling network. However, if the grid contains harmonics, these harmonics will also occur in the fundamental synchronous reference frame d and q components. For example, the positive sequence component of the third harmonic occurs as a 100 Hz component in $U_d^+$ while the negative sequence component of the third harmonic appears as a 200 Hz component, respectively. The same way, the positive sequence of the second harmonic occurs as 50 Hz component and the negative sequence of the second harmonic arises as 150 Hz component in $U_d^+$. However, the low-pass filters used after the DDSRF blocks filter out also these harmonics resulting in only the DC values of the fundamental component to get through to output.

### 4.2.2 Synchronous fundamental dq-frame

A common way to do harmonics compensation with the help of synchronous reference frame is so called fundamental dq-frame method. As mentioned before, harmonics occur as oscillations in the synchronous reference dq-frame. In other words, d and q components consist of DC and AC components. In fundamental dq-frame method, the idea is to extract the AC component as it is the harmonics part of the dq signal. [29, 30] Figure 22 illustrates the idea of the fundamental dq-frame method.

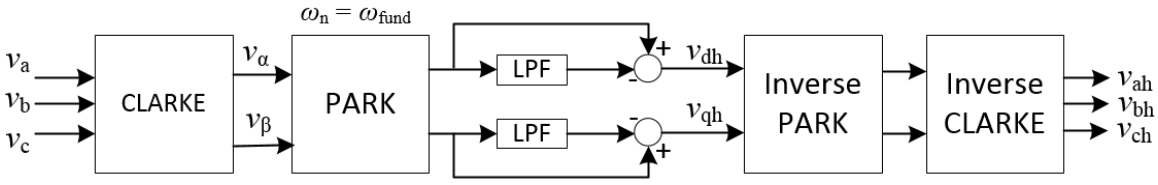


***Figure 22.*** *Harmonics detection with fundamental dq-frame method.*

As can be seen in Figure 22, at first the Park transformation is done to get $v_d$ and $v_q$ of the fundamental frequency. These two components consist of DC and AC components when the input signals contain harmonics. The DC parts are extracted with low-pass filters and then subtracted from $v_d$ and $v_q$ resulting only the AC components to be taken further to the inverse Park transformation. These components are presented in Figure 22 as $v_{dh}$ and $v_{qh}$. This way, after the inverse Park and the inverse Clarke transformations, the output signals contain only harmonics which thus can be fed forward to cancel out the grid harmonics. All in all, the fundamental dq-frame method gives the whole harmonic spectrum as its output. If a selective harmonics detection and compensation is wanted then the fundamental dq-frame method is not the right choice. [30]

### 4.2.3 Synchronous harmonic dq-frame

In a harmonic dq-frame method, harmonics detection can be done selectively unlike in the fundamental dq-frame method. The harmonic dq-frame uses individual dq-frames for each harmonic component. In other words, each harmonic dq-frame rotates with an angular speed equal to a specific harmonic. Otherwise the principle of this method is very similar with the fundamental dq-frame method. For example, for the third harmonic a dq-frame rotating at 150 Hz is implemented. Thus, $v_d$ and $v_q$ in this reference frame contain the third harmonic as a DC component and other harmonics as well as the fundamental frequency as an AC component. The detection of the specific harmonic component can therefore be done by removing the AC component with a low-pass filter similar with the fundamental dq-frame method. [29, 30] The principle of the harmonic dq-frame for a detection of the 3$^{rd}$, 5$^{th}$ and 7$^{th}$ harmonics is illustrated in Figure 23.

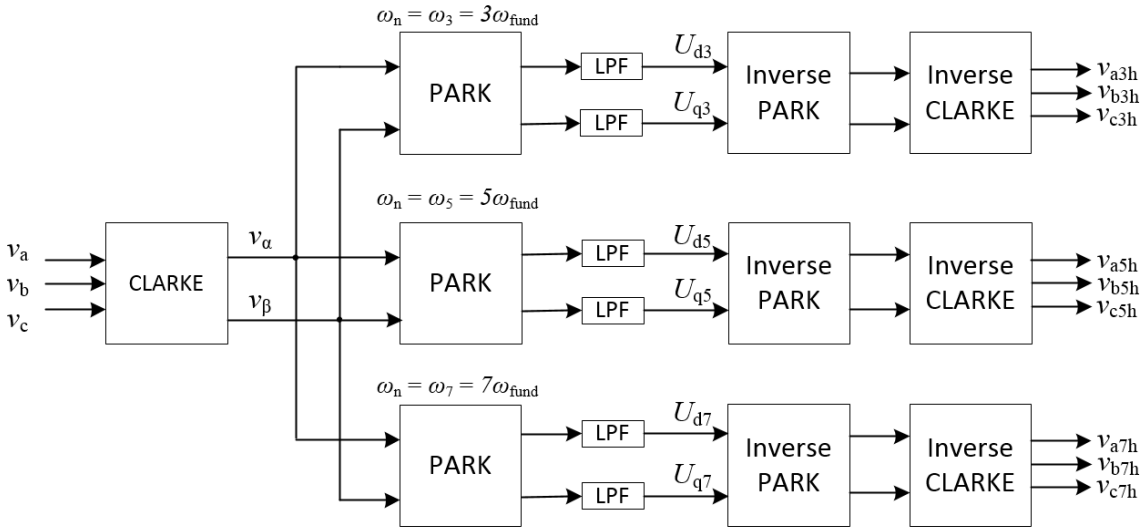


***Figure 23.*** *Detection of the 3rd, 5th and 7th harmonics with the harmonic dq-frame method.*

As can be seen in Figure 23, each synchronous reference frame rotates according to a specific harmonic frequency thus making the wanted harmonic to appear as a DC component after the Park transformation. Low-pass filters are used to remove the AC components as explained earlier. The phase angle needed for each Park transformation is taken from the PLL based on the fundamental frequency dq-frame. This angle is scaled by a coefficient which consequently determines the order of the harmonic to be detected. As a result, after low-pass filters and the inverse Park and Clarke transformations, harmonic components in the natural abc reference frame are provided as outputs. [29, 30] However, as the conventional PLL is prone to inaccuracy when the grid contains a great number of harmonics, a bandpass filter can be used to let only the fundamental frequency component pass through to the fundamental SRF-PLL block. Thus, the accuracy of the synchronization angle increases and the error especially for higher frequency dq-frames decreases. This harmonic dq-frame method can be extended by adding new harmonic dq-frames for all harmonics that need to be detected and compensated. Moreover, the harmonic dq-frame method can be upgraded by using individual DDSRF blocks to enable positive-negative sequence detections of different harmonics.

The low-pass filter has zero phase shift for DC components and thus the harmonic dq-frame doesn't have the issue with the phase shift because of the low-pass filter as the harmonic component occurs as a DC component after the Park transformation. However, as the fundamental frequency component is significantly larger compared to harmonic components the output of the Park transformation occurs to have a substantial AC component. As a result, the cut-off frequency of the low-pass filter needs to be set very low to eliminate the impact of this AC component. This on the other hand leads to degraded response time. To overcome this issue a cross-feedback network, a plain version of the cross-feedback network used with MSOGI, is developed. Simply, a fundamental dq-

frame can be used to detect the fundamental frequency component which then is converted to the stationary reference frame (αβ components) and subtracted from the input signal. Thus, the input signals of each harmonic Park transformation block won't contain the fundamental frequency component anymore. Respectively, the outputs of each Park transformation block won't contain a significant AC component and furthermore the cut-off frequency of the low-pass filter can be set in a way to achieve an acceptable response time.

As it was with MSOGI, the reference vectors in the control system need to be phase shifted to neutralize the effects of the star-delta connected transformer, delta connected STATCOM as well as the grid impedance angle. The phase shifting can be done with a rotation matrix in the αβ-frame similar with the method used in SOGI. However, the needed phase shift is possible to be implemented correspondingly in a harmonic dq-frame. The d and q components can be converted from rectangular form to polar form as presented in equations 37 and 38.

$$Mag = \sqrt{U_d^2 + U_q^2} \tag{37}$$

$$Ang = tan^{-1}\left(\frac{U_q}{U_d}\right) \tag{38}$$

The above equations provide magnitude and angle in the harmonic dq-frame and thus the phase shift can easily be implemented in polar form by summing up the polar form angle and the needed phase shift. Polar coordinates can then be converted back to rectangular form i.e. back to d and q components. The presented method to implement the phase shift in the dq-frame is easy to understand and thus practical. However, the most optimal solution to implement the required phase shift is to do it by simply rotating the dq-frame coordinate system. In other words, by adding the wanted phase shift to the synchronization angle before the inverse Park transformation the reference vector can be rotated by using only one sum operator.

The harmonic dq-frame method is widely used in active filter applications due to well-covered literature of the dq-theory and the possibility to selectively control separate harmonics [29]. Moreover, the control can be done by using DC values which makes the whole control design simpler. In this thesis, the harmonic dq-frame method is further studied i.e. used in simulations as it is capable of selective harmonics detection which is wanted.

# 5. SIMULATIONS

In this chapter, simulations are done for the MSOGI based method and for the synchronous harmonic dq-frame method (later SRF based method). The studied methods are implemented into an existing STATCOM simulation model in PSCAD environment where the simulations are correspondingly carried out. The simulation model consists of an ideal grid voltage source, a separate series connected harmonic voltage source, grid impedance, a wye-delta connected transformer and the actual STATCOM system. In a simplified single line diagram, presented in Figure 24, the ideal grid voltage source and the series connected harmonic voltage source are presented as a single grid voltage source.

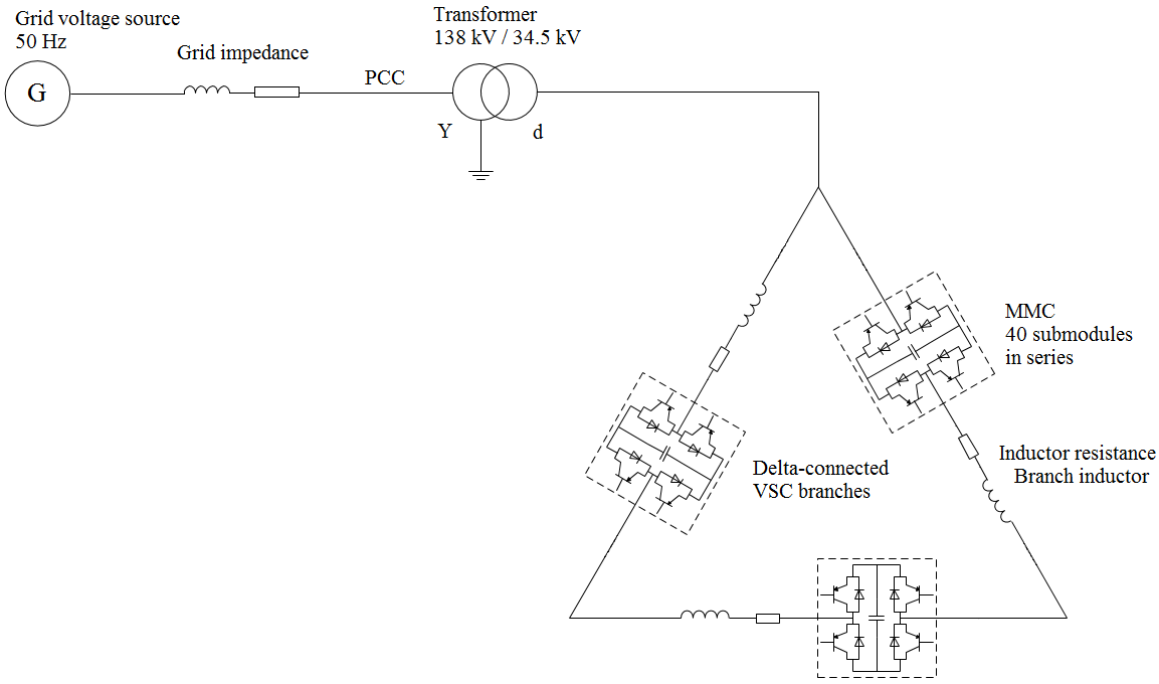


***Figure 24.*** *Simplified single line diagram of the circuit used for simulations.*

In the simulation model, STATCOM is modelled as a voltage source converter whose three-phase voltages are produced by a control system. The actual simulation model includes several parts not shown in the single line diagram. However, those are not relevant for the understanding of this work. In general terms, in this thesis, harmonics compensation is done by measuring the phase voltages at the point of common coupling (PCC), detecting harmonics with the help of studied methods and by creating a reference current that together with the reactive power compensation reference current produces the wanted VSC voltage and thus the wanted actual compensation current. The harmonic compensation reference current in the control system with the MSOGI based method is created from the detected voltage harmonics by a PR-controller already existing in the used simulation model. Respectively, with the SRF based method, the corresponding reference

current is created from the detected voltage harmonics by a simple integrator (I-controller). Tunings of the controllers are not further considered in this thesis as only simulations in steady-state cases are done. Also, the control of the entire STATCOM system is not considered in more detail as the basic understanding of the operation is enough regarding this thesis.

In this thesis, odd harmonics up to 15$^{th}$ harmonic order are to be compensated. Thus, the implemented MSOGI based method consists of eight DSOGI blocks, seven blocks for harmonics and one for the fundamental, with a corresponding cross-feedback network and the implemented SRF based method of seven harmonic dq-frames and one fundamental dq-frame, respectively.

## 5.1 Simulation settings

In the first simulations, the harmonic voltage source is set to generate odd harmonics up to 15$^{th}$ harmonic according to Table 3.

***Table 3.*** *Grid harmonics for the first simulations.*

| Harmonic order | 3 | 5 | 7 | 9 | 11 | 13 | 15 |
|---|---|---|---|---|---|---|---|
| Harmonic voltage % of the fundamental | 2 | 2 | 2 | 2 | 2 | 2 | 2 |

Other harmonics are set to zero. This is to get reference how each method performs when the grid contains only harmonics the active filter is set to compensate. Standard IEC 61000-3-6 presents indicative planning levels for harmonic voltages up to 50$^{th}$ harmonic. The planning levels were presented in Table 2 earlier. These planning levels are used in later simulations to create appropriate number of harmonics in the grid to demonstrate the performance in real life situation. The voltage THD calculated from the individual harmonic limits is 5.33 %. However, standard IEC 61000-3-6 also presents indicative level of 3 % for total harmonic distortion which thus will not be met if the grid harmonics are set according to individual harmonic limits. Harmonics are thus scaled by a factor of 0.55 to meet the presented voltage THD. The standard defines only harmonic limits up to 50$^{th}$ harmonic but not above. However, the grid is wanted to contain also higher order harmonics and thus voltage magnitude of 0.1 % of the fundamental component is added for harmonic orders between 51 and 100. The resulting voltage THD is 3.015 %. The angles of the harmonics in respect to the fundamental voltage angle are set to zero degrees. The used harmonic spectrum is presented in Figure 25.

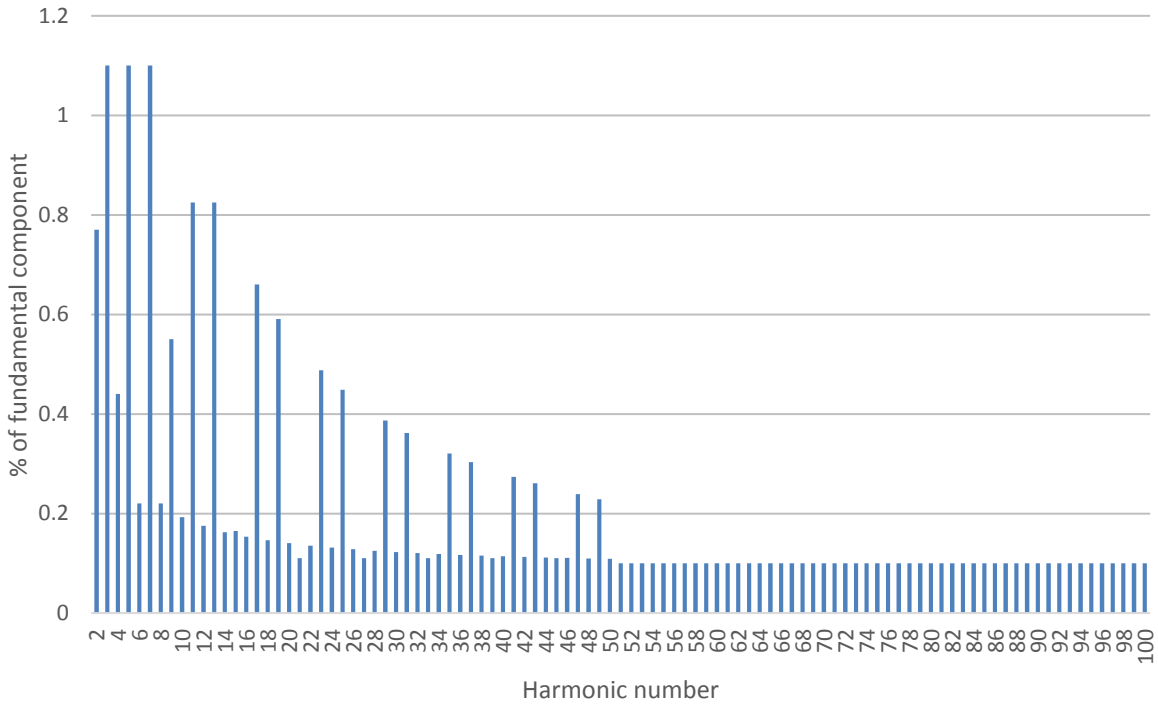


***Figure 25.*** *Voltage harmonic spectrum used for background distortion.*

The grid harmonics are generated by the harmonic voltage source in the grid. Harmonic spectrums at PCC will be different as the simulation model has grid impedance between the harmonic voltage source and PCC.

Simulation results are realized by extracting harmonics from measured waveforms with a Fast Fourier Transform block in PSCAD and further by exporting data to Excel for calculations and graph drawing. Relevant system parameters for the simulations are presented in Appendix A.

## 5.2 Performance of the MSOGI method

In this subchapter, the performance of the studied MSOGI based active filter method is simulated in steady-state cases. Simulations are done to demonstrate the performance of the MSOGI based method in case of positive and negative sequence harmonics, in STATCOM's different operation points and under highly distorted circumstances.

### 5.2.1 Positive and negative sequence filtering with MSOGI

The first two simulations are done to perceive how well MSOGI performs when the grid contains mostly the harmonics MSOGI is set to compensate. STATCOM's reactive power compensation is at first set to the zero-operation point to narrow down its possible effects on the active filtering. For the first simulation the harmonic source in the grid is set to generate only positive sequence odd harmonics up $15^{th}$ harmonic according to Table 3. The corresponding harmonic spectrum at PCC can be seen in Figure 26.

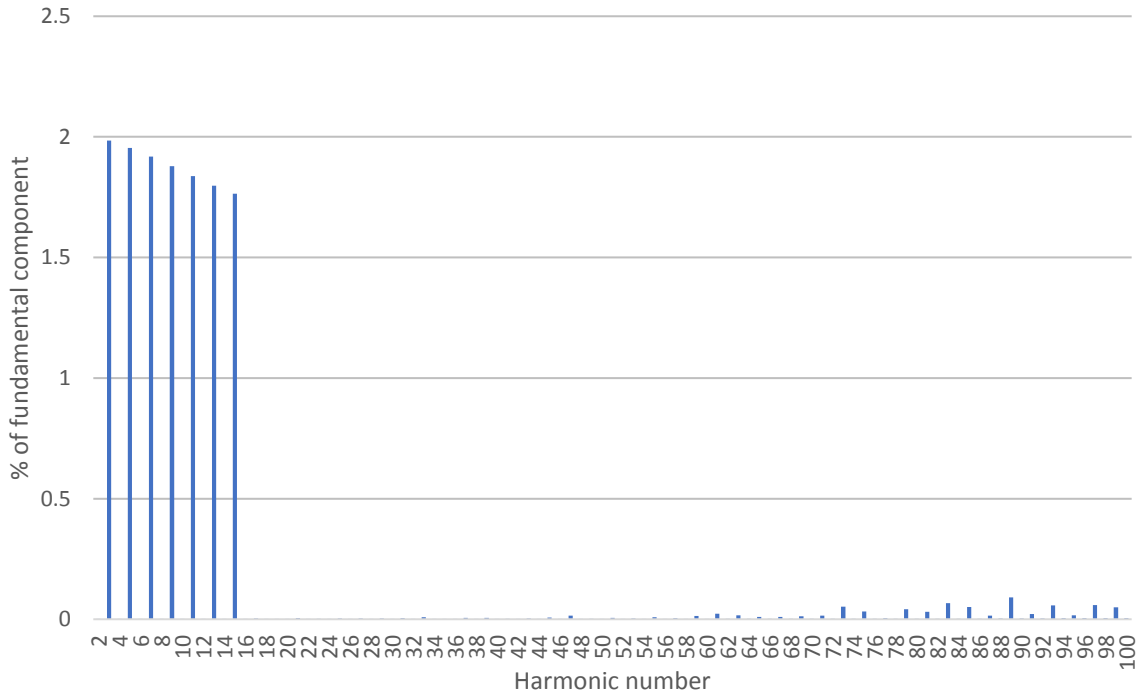


***Figure 26.*** *Harmonics at PCC in case of odd harmonics up to 15th in the grid are positive and the MSOGI based active filter is not in use.*

Harmonic spectrum is shown all the way up to 100$^{th}$ harmonic to ensure the active harmonic filter will not only compensate the harmonics it is set to compensate but also that it will not significantly increase other harmonics while compensating. Harmonics at PCC are lower compared to the values set for the harmonic voltage source in the grid. This is naturally due to inductive grid impedance between the voltage source and PCC that linearly increases as a function of increasing frequency causing different amount of voltage drop to occur for different harmonics. Also, even though the harmonic source is set to generate only odd harmonics up to 15$^{th}$ harmonic, other harmonics can still be noticed to occur at PCC. This is due to STATCOM's normal operation when creating the fundamental voltage component even at its zero-operation point. Voltage THD at PCC before harmonics control is enabled is 4.9720 %. Figure 27 shows the final harmonic spectrum at PCC when the active filter is given enough time to control the grid harmonics to the smallest possible.

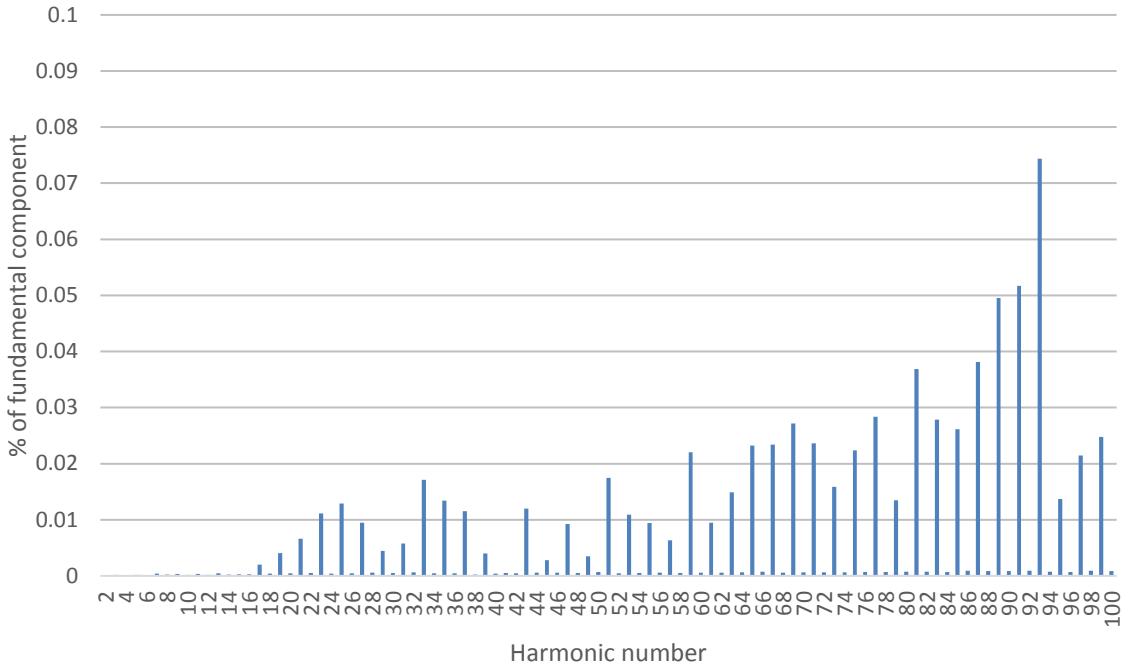


***Figure 27.*** *Harmonics at PCC in case of odd harmonics up to 15th in the grid are positive and the MSOGI based active filter is in use.*

As can be seen in Figure 27, the controlled harmonics settle down very close to zero. Moreover, even if some variety in other harmonics may be seen, no significant increase in individual harmonic components is still noticed. The final voltage THD at PCC is 0.1518 % which implies the voltage waveform to be almost an ideal sinewave. Figure 28, furthermore, presents the PCC voltage waveforms in time domain before the active harmonic filter control is enabled and after the grid harmonics have been compensated to the smallest possible.

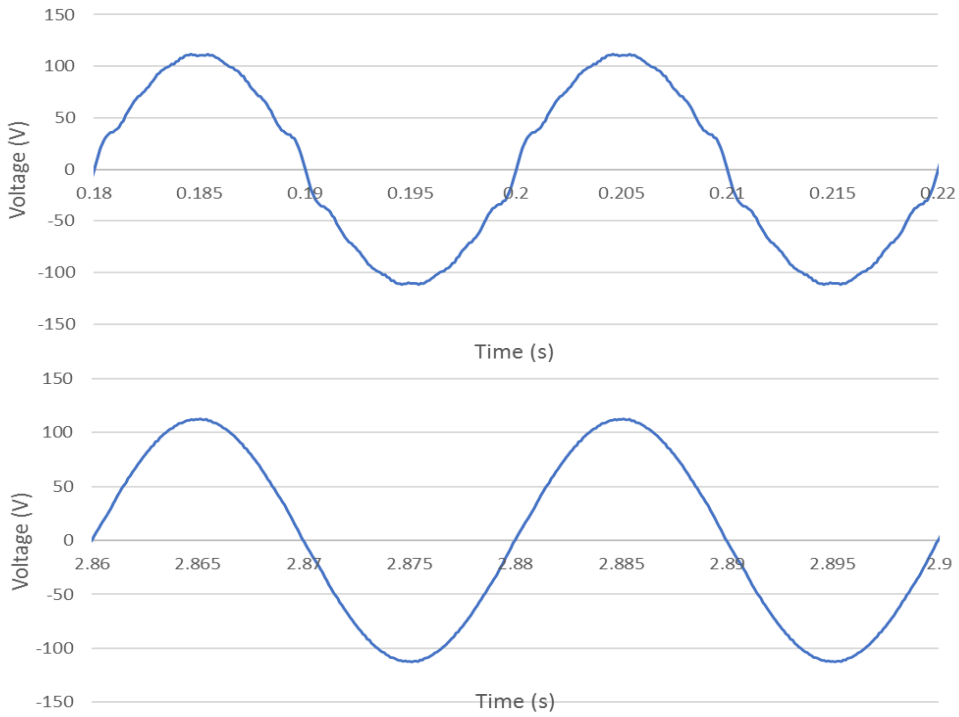


***Figure 28.*** *Voltage waveform at PCC before and after active filtering.*

As can be seen in Figure 28, the final voltage waveform is noticeably less distorted compared to the initial voltage waveform after harmonics have been compensated. To further illustrate the real-time active filtering, Figure 29 presents the compensation of the 7$^{th}$ harmonic as a function of time.

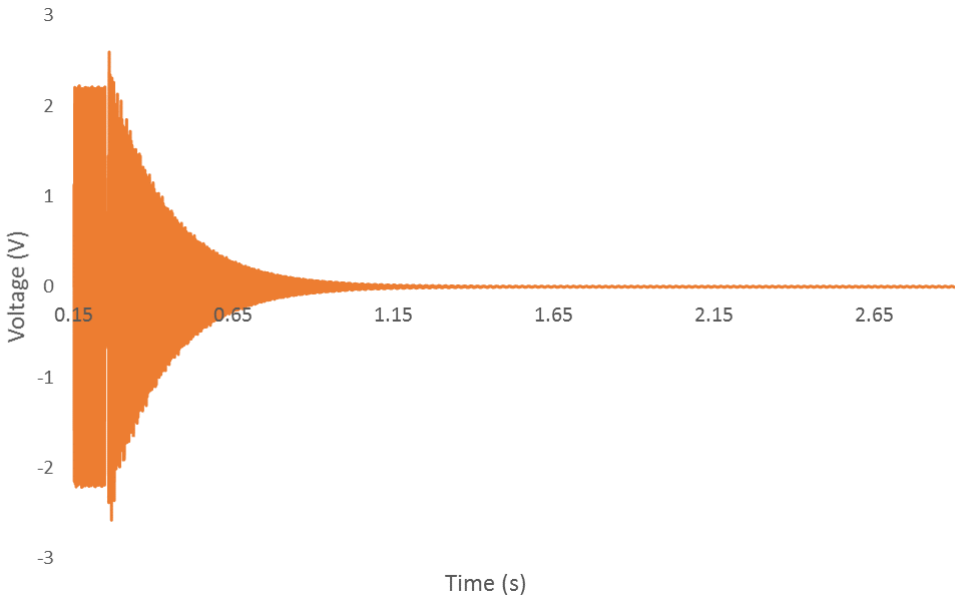


***Figure 29.*** *Filtering of the 7th harmonic.*

As can be seen in Figure 29, the 7$^{th}$ harmonic decreases smoothly after active filter control is enabled (t = 0.25 s) and in the end, settles down to zero as perceived also before.

The second simulation is similar to the previous one but the harmonic source in the grid is set to generate only negative sequence harmonics instead of positive sequence harmonics. STATCOM is set to still operate at the zero-operation point. The corresponding harmonic spectrum at PCC is shown in Figure 30.

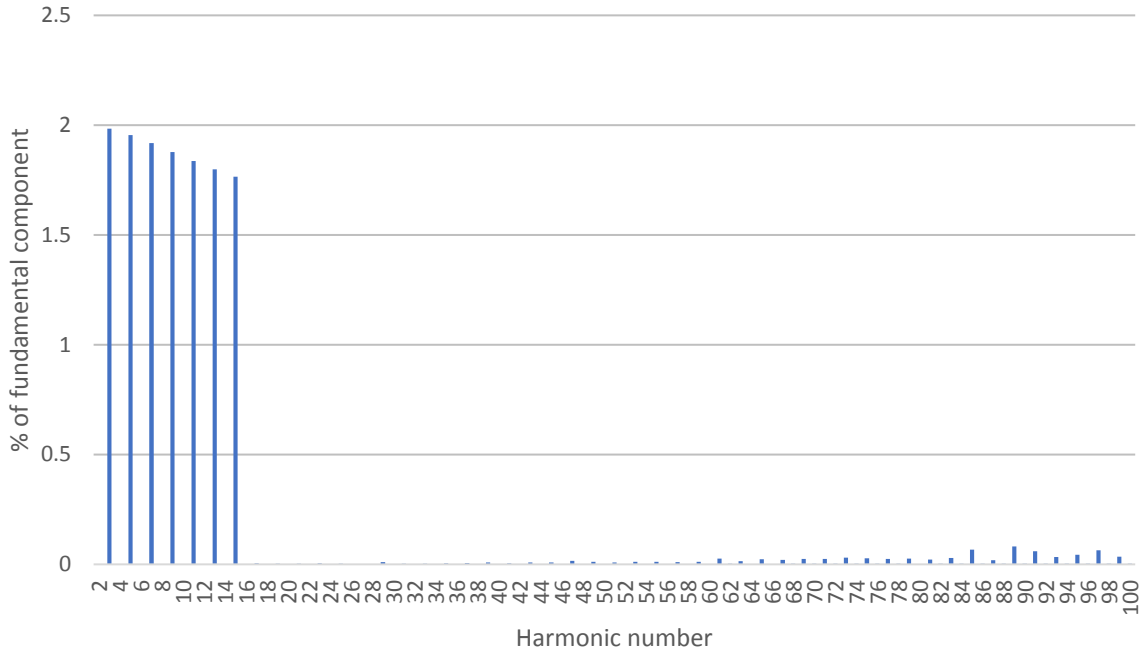


***Figure 30.*** *Harmonics at PCC in case of odd harmonics up to 15th in the grid are negative and the MSOGI based active filter is not in use.*

THD at PCC before the active filter feature is enable is 4.9720 % which is the same as in the previous case. Figure 31 shows the final harmonic spectrum at PCC when the active filter is given enough time to control the grid harmonics to its minimum.

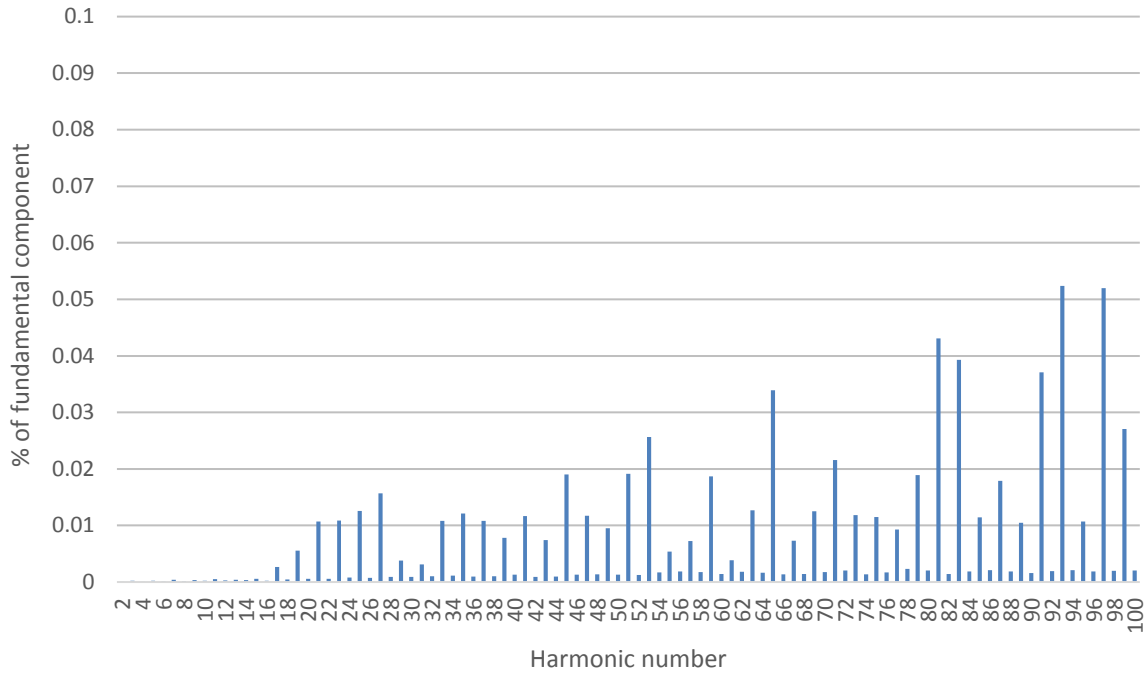


***Figure 31.*** *Harmonics at PCC in case of odd harmonics up to 15th in the grid are negative and the MSOGI based active filter is in use.*

As can be seen in Figure 31, the controlled harmonics settle down again very close to zero and similar to the first simulation no significant increase in other harmonics is noticed. The final THD at PCC is 0.1335 % that is close to the final THD in the positive sequence case. As a result, MSOGI can be considered to perform the same way for both positive and negative sequence harmonics. The next simulations are done by using only positive sequence harmonics to decrease the number of simulations.

### 5.2.2 MSOGI under distorted circumstances

To test MSOGI's performance under highly distorted circumstances the harmonic source in the grid is set to generate harmonics according to standard's IEC 61000-3-6 planning levels. STATCOM is at first set to operate at its zero-operation point similar to the previous simulations and later set to its maximum capacitive and maximum inductive operation points. The harmonic source in the grid is set to generate only positive sequence harmonics. The corresponding harmonic spectrum at PCC before the active filter control is enabled is presented in Figure 32.

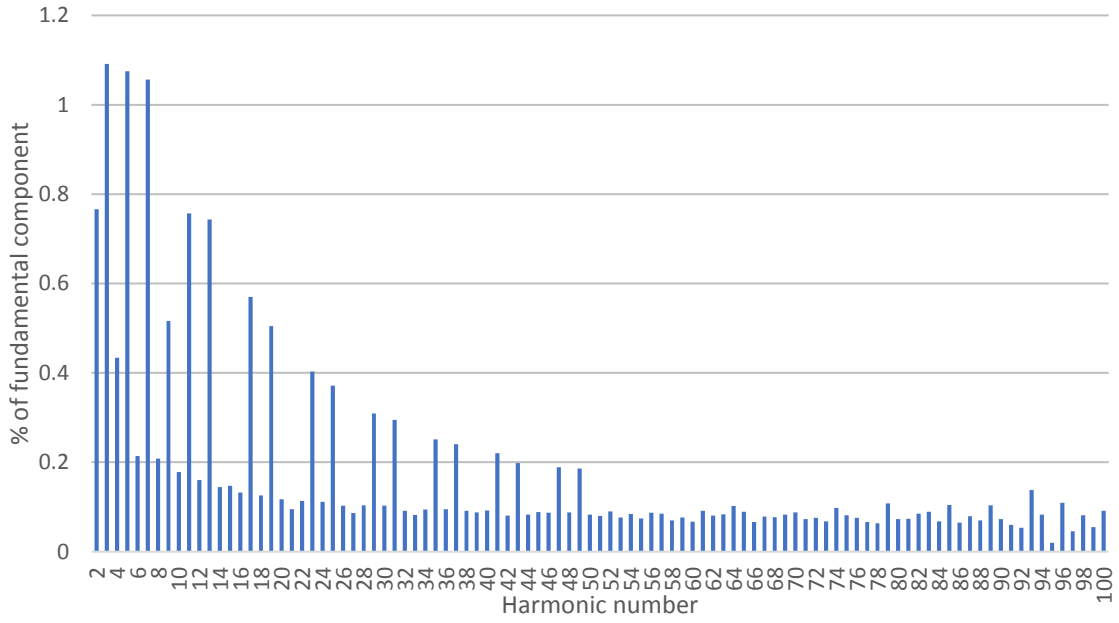


***Figure 32.*** *Harmonics at PCC in case of positive sequence harmonics set up to 100th according to IEC 61000-3-6 and the MSOGI based active filter is not in use.*

THD at PCC is 2.7772 %. Figure 33 shows the final harmonic spectrum at PCC after the active filter control is enabled and it is given enough time to control the grid harmonics to the smallest possible.

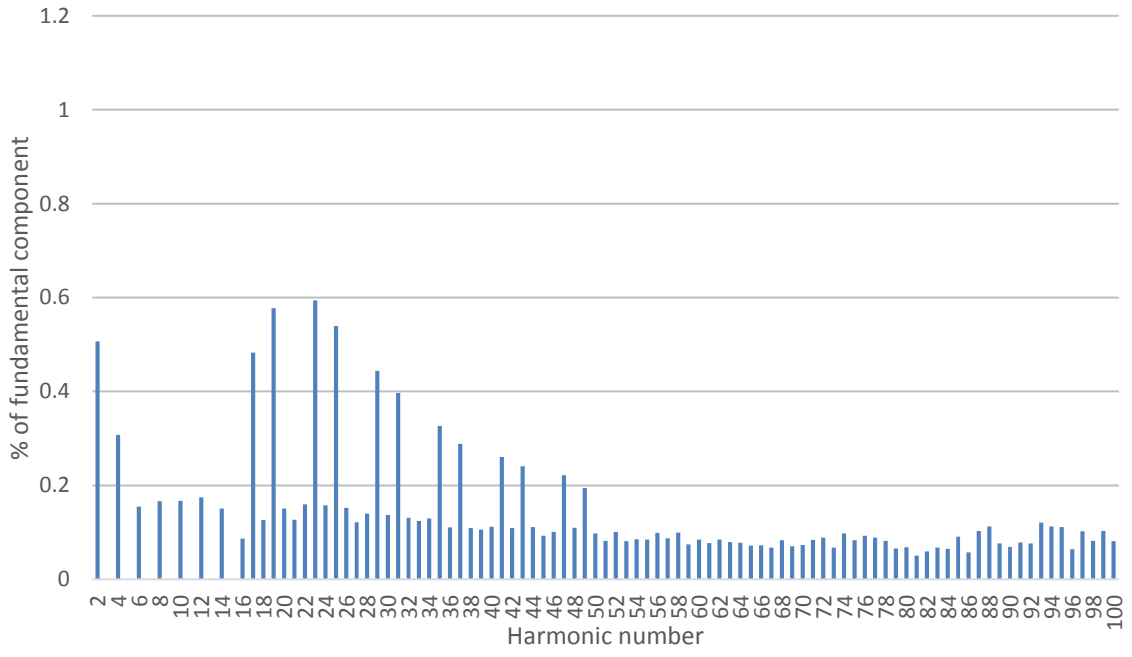


***Figure 33.*** *Harmonics at PCC in case of positive sequence harmonics set up to 100th according to IEC 61000-3-6 and the MSOGI based active filter is in use.*

As can be seen in Figure 33, the controlled odd harmonics settle down very close to zero even when the grid contains a great number of other harmonics. Some increase can be

seen in other harmonics with the maximum increase of 0.16 % at the 23rd harmonic but overall no significant increase is still noticed. Final THD at PCC is 1.7765 % which is considerably smaller than the initial THD at PCC (2.7772 %).

As the active harmonic filter feature is meant to operate simultaneously with the reactive power compensation, simulations at the maximum capacitive and at the maximum inductive operation points should be performed. Simulation settings are otherwise similar with the previous simulation but now STATCOM's reactive power compensation is set to its maximum capacitive operation point. The corresponding harmonic spectrum at PCC can be seen in Figure 34.

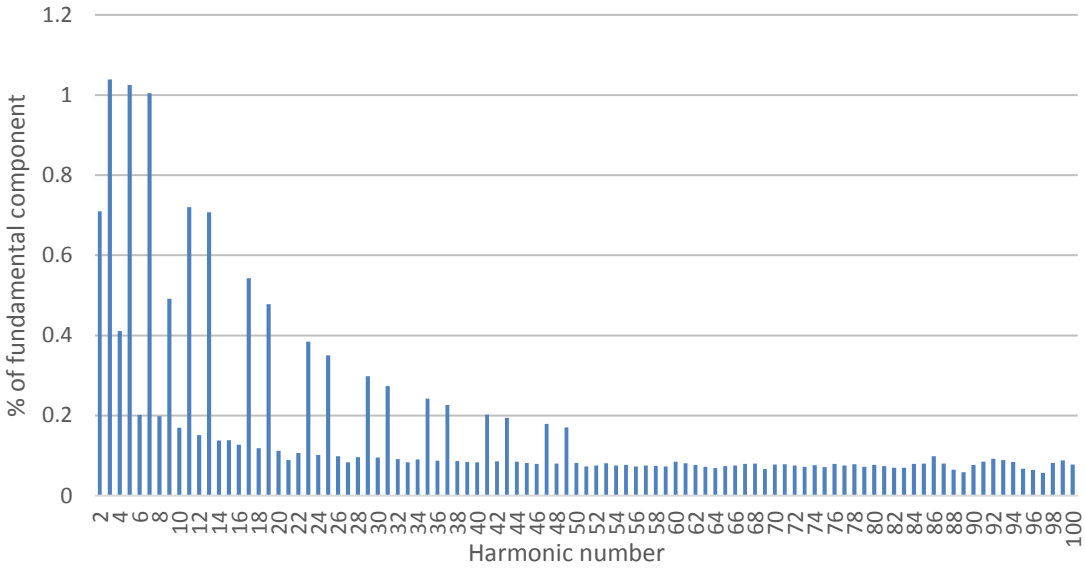


***Figure 34.*** *Harmonics at PCC in case of STATCOM operating at its maximum capacitive operation point and the MSOGI based active filter is not in use.*

THD at PCC before the active filter control is enabled is 2.6342 %. As can be seen in Figure 34, harmonics tend to be smaller in terms of percentage of the fundamental component compared to the previous case when STATCOM's reactive power compensation was set to the zero-operation point. This is due to the capacitive power compensation which increases the fundamental voltage at PCC resulting in harmonic components to be smaller in terms of percentage. The relation between the grid voltage and the PCC voltage can be presented according to Kirchhoff's voltage law as follows:

$$V_{GRID} = V_{PCC} + Z_{GRID} I_Q, \tag{39}$$

where $V_{GRID}$ is the grid voltage, $V_{PCC}$ is the voltage at PCC, $Z_{GRID}$ is the grid impedance and $I_Q$ is the reactive current produced by STATCOM. In Figure 35 phasor diagrams for capacitive and inductive operations points are illustrated based on equation 39. The grid impedance is assumed to be purely inductive to simplify drawings.

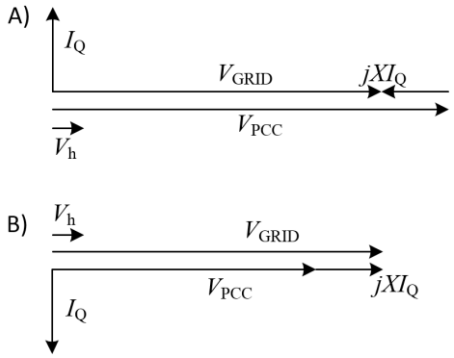


***Figure 35.*** *The impact of A) capacitive and B) inductive current to PCC voltage.*

As can be seen in Figure 35A), when STATCOM generates capacitive current, it leads to an increase in the fundamental $V_{PCC}$ magnitude. However, harmonic voltages $V_h$ remain the same at PCC which thus results in them to appear smaller in terms of percentage compared to the results when STATCOM was operated at its zero-operation point. Respectively, when STATCOM is operated at the inductive side, the fundamental $V_{PCC}$ magnitude decreases as can also be noticed in Figure 35B). Naturally, as absolute values of harmonic voltages remain the same, the harmonic voltages appear to be greater in terms of percentage compared to STATCOM's zero-operation and capacitive operation results.

Figure 36 shows the final harmonic spectrum after enough time is given for the active filter control to compensate the grid harmonics to its minimum.

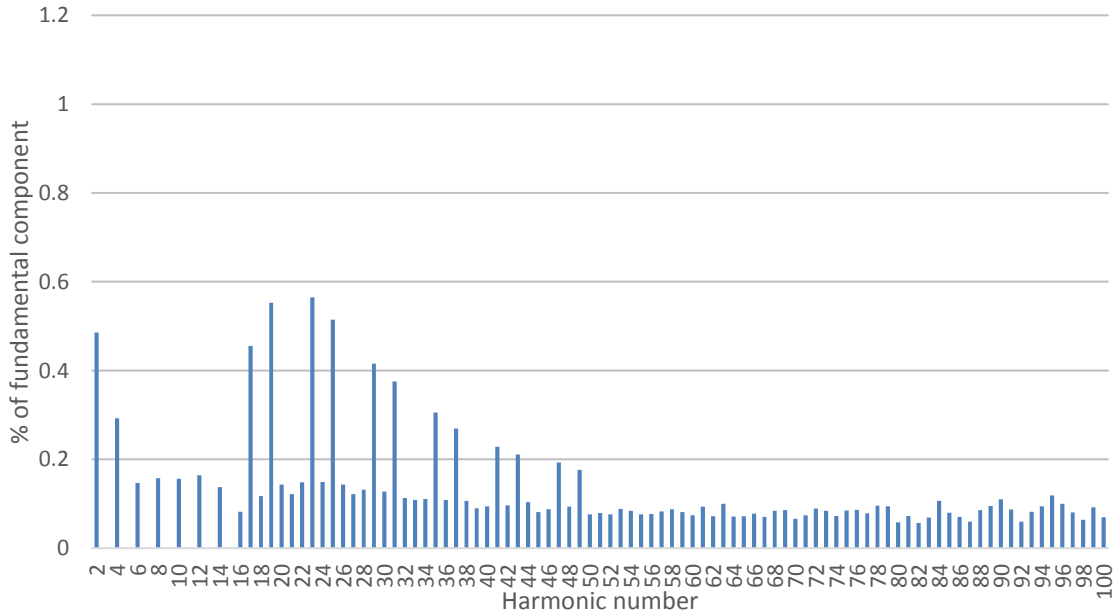


***Figure 36.*** *Harmonics at PCC in case of STATCOM operating at its maximum capacitive operation point and the MSOGI based active filter is in use.*

As can be seen in Figure 36, the controlled odd harmonics settle down very close to zero also when operating in the maximum capacitive operation point. Final THD at PCC is

1.6773 % that is slightly smaller than earlier when STATCOM's reactive power compensation was set to zero-operation point. This, however, can be explained by the nature of capacitive power compensation that increases the fundamental voltage at PCC as mentioned before. Absolute values of harmonic components are still very close to the same.

Finally, the MSOGI based active filter feature is simulated in STATCOM's maximum inductive operation point. The corresponding harmonic spectrum at PCC is shown in Figure 37.

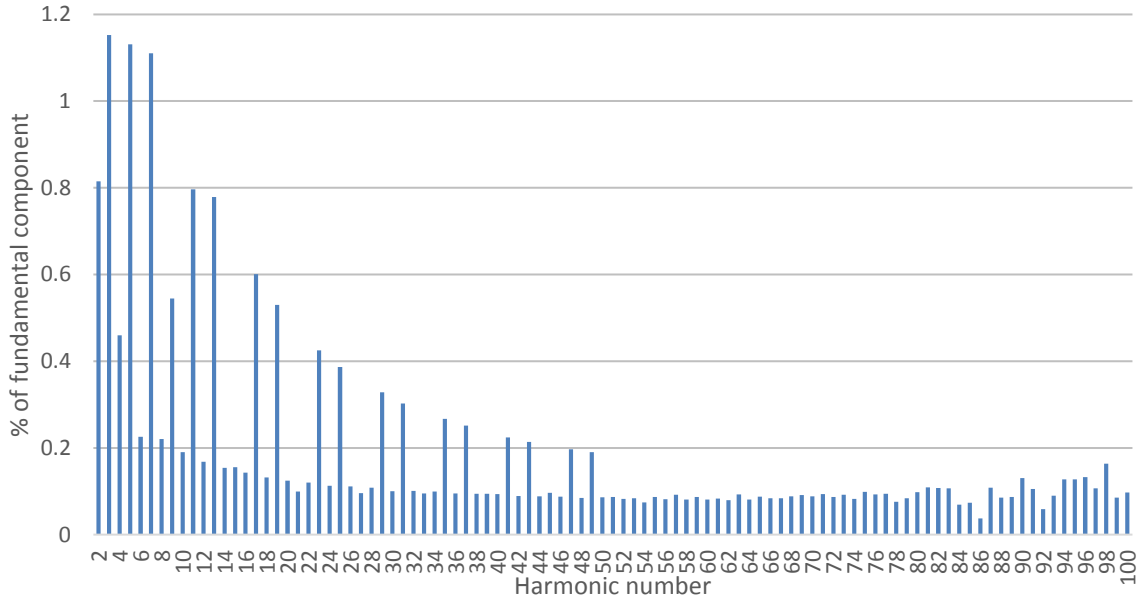


***Figure 37.*** *Harmonics at PCC in case of STATCOM operating at its maximum inductive operation point and the MSOGI based active filter is not in use.*

THD at PCC before the active filter control is enabled is 2.9376 %. As predicted, harmonics are mainly larger in terms of percentage than in previous cases due to inductive power compensation. Figure 38 shows the final harmonic spectrum after enough time is given for the active filter control to compensate the grid harmonics to the smallest possible.

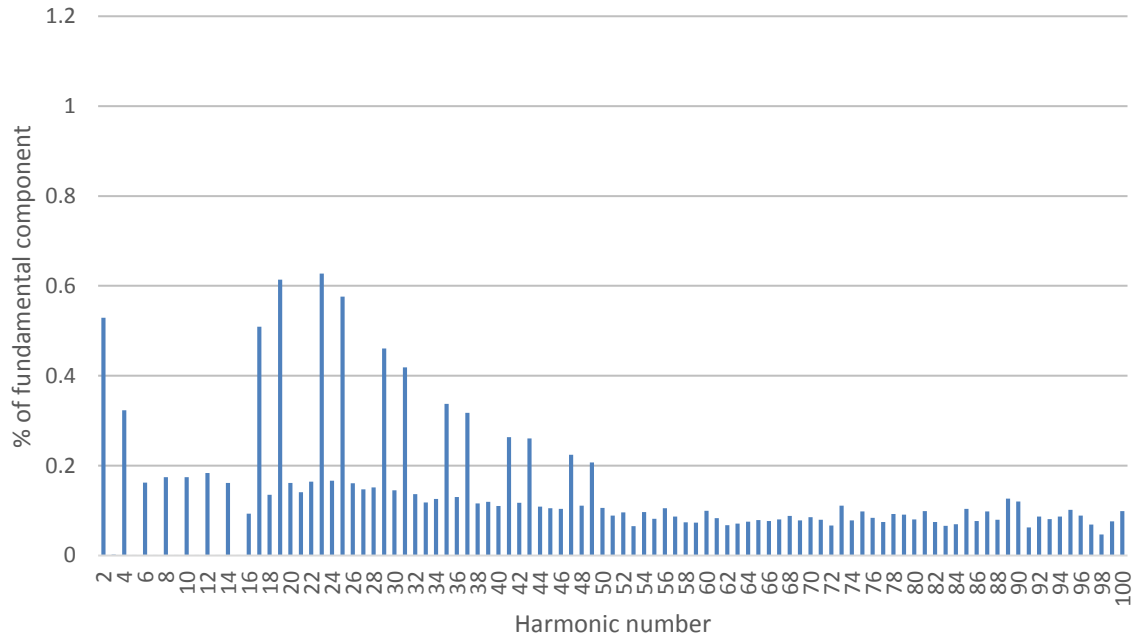


***Figure 38.*** *Harmonics at PCC in case of STATCOM operating at its maximum inductive operation point and the MSOGI based active filter is in use.*

As can be seen in Figure 38, the controlled odd harmonics settle down very close to zero as well when operating at the maximum inductive operation point. Final THD at PCC is 1.8679 % that is greater than earlier when STATCOM was set to operate at its maximum capacitive operation point (1.6773 %). The greater final THD can be explained by the nature of inductive power compensation that decreases the fundamental voltage component at PCC. Absolute values of harmonic components are thus very close to those when STATCOM was operated at its capacitive and zero-operation points. The decrease from the initial THD at PCC can also be considered significant.

The MSOGI based active filter method can be considered to operate properly in all three operation points simulated (zero-operation, maximum capacitive and maximum inductive) even when the grid contains a great number of other harmonics.

## 5.3 Performance of the SRF based method

In this subchapter, the performance of the studied harmonic dq-frame based (SRF based) active filter method is simulated in steady-state cases. Simulations are done to demonstrate the performance of the SRF based method in case of positive and negative sequence harmonics, in STATCOM's different operation points and under highly distorted circumstances. The simulations are analogous with the simulations done with MSOGI.

### 5.3.1 Positive and negative sequence filtering with SRF

The first simulations for the SRF based method are done to observe how well harmonics can be compensated when the grid contains only the harmonics SRF based active filter is set to compensate. The harmonic compensation shouldn't either generate significantly any other harmonics to the grid. At first, the harmonic voltage source in the grid is set to generate only positive sequence odd harmonics up to 15$^{th}$ harmonic to the grid according to Table 3. STATCOM is set to operate at its zero-operation point. The harmonic spectrum at PCC before harmonic compensation is enabled is similar with the spectrum presented earlier in Figure 26. The harmonic spectrum after the SRF based active filter control is given enough time to control the harmonics to its smallest possible is shown in Figure 39.

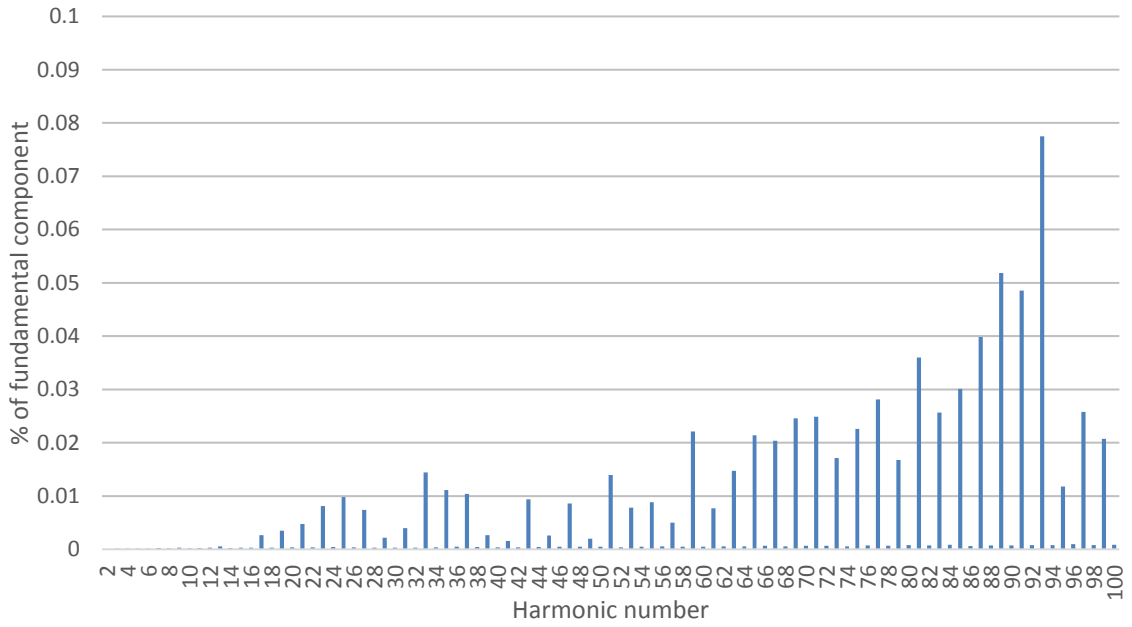


***Figure 39.*** *Harmonics at PCC in case of odd harmonics up to 15th in the grid are positive and the SRF based active filter is in use.*

As can be seen in Figure 39, the controlled odd harmonics settle down very close to zero. The final values of the controlled harmonics are almost equal with the results got with MSOGI. Also, the absolute values of other harmonics are very close to those with MSOGI i.e. no significant increase in uncontrolled harmonics can be noticed. The final THD at PCC settles down to 0.1508 % which is thus almost identical with the final THD got with MSOGI (0.1518 %).

The second simulation is done by setting the harmonic source in the grid to generate only negative sequence odd harmonics up to 15$^{th}$ harmonic instead of positive sequence harmonics. Otherwise the simulation is similar with the previous one. The harmonic spectrum at PCC before the active filter control is enabled is similar with the spectrum presented earlier in Figure 30. The final harmonic spectrum at PCC after the SRF based

active filter control is given enough time to control the harmonics to the smallest possible is presented in Figure 40.

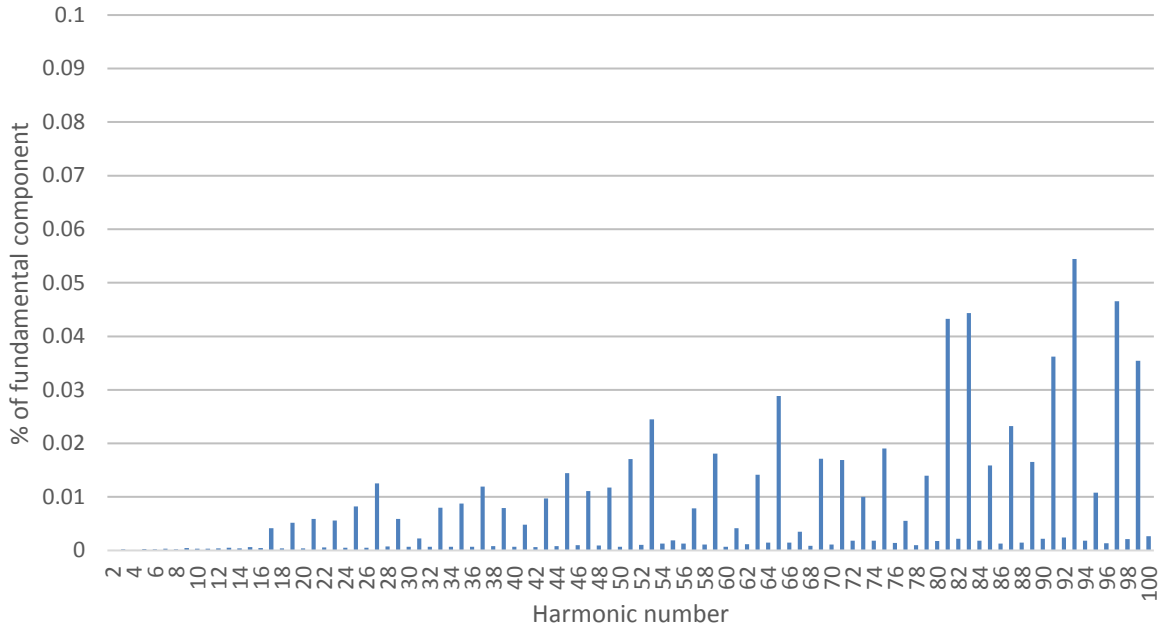


***Figure 40.*** *Harmonics at PCC in case of odd harmonics up to 15th in the grid are negative and the SRF based active filter is in use.*

The controlled harmonics settle down again very close to zero as can be seen in Figure 40. The final values of controlled harmonics are almost identical with the results got with MSOGI. Similar to the previous simulation, no significant increase either in other harmonics can be noticed. The final THD at PCC settles down to 0.1331 % which is again practically the same as the final THD got with MSOGI (0.1335 %). The SRF based active filter feature can be stated to perform almost similarly for both positive and negative sequence harmonics. As a consequence, the next simulations are done by using only positive sequence harmonics to reduce the number of simulations.

### 5.3.2 SRF under distorted circumstances

To test SRF based active filter feature under distorted circumstances the harmonic source in the grid is set to generate harmonics according to standard's IEC 61000-3-6 planning levels. STATCOM is at first set to operate at its zero-operation point similar to previous simulations and then set to its maximum capacitive and maximum inductive operation points. The harmonic source in the grid is set to generate only positive sequence harmonics. The harmonic spectrum at PCC before the active filter control is enabled is similar with the spectrum presented earlier in Figure 32. The final THD at PCC after the active filter control is given enough time to control the grid harmonics to the smallest possible is presented in Figure 41.

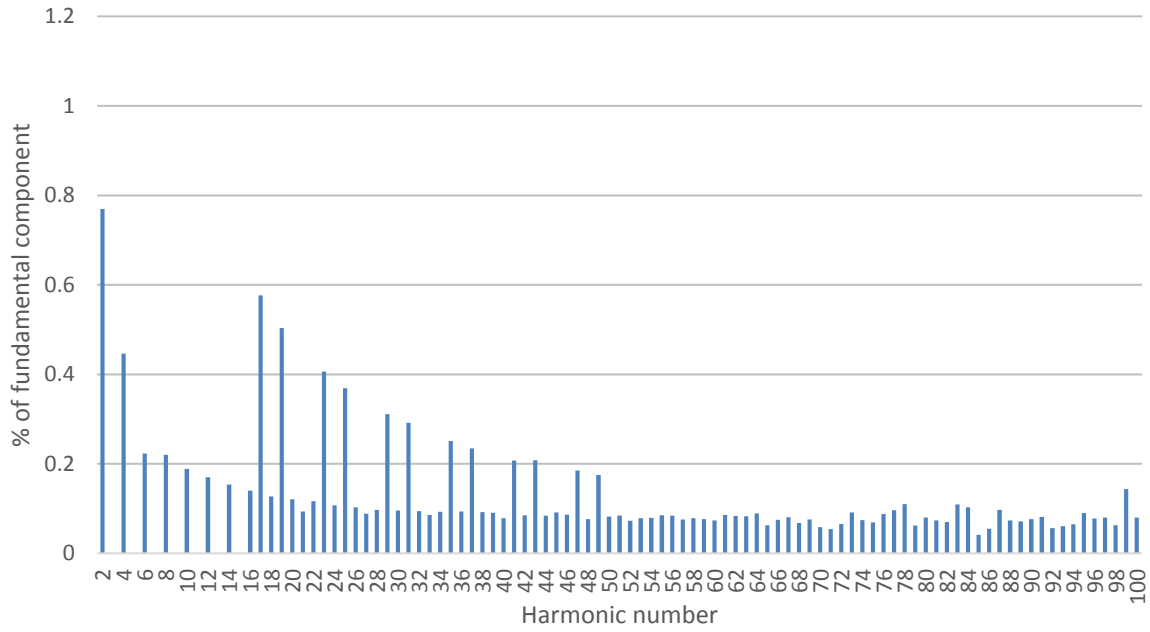


***Figure 41.*** *Harmonics at PCC in case of positive sequence harmonics set up to 100th according to IEC 61000-3-6 and the SRF based active filter is in use.*

As can be seen in Figure 41, all the controlled harmonics decrease to zero even when the grid contains a great number of other harmonics. The final values of the controlled harmonics are very close to the corresponding final values got with MSOGI and thus the SRF based method can be considered capable of compensating selected harmonics practically completely. The uncontrolled harmonics remain very close to the initial situation with only some variety. The final THD at PCC settles down to 1.6895 % which is roughly 0.1 % smaller than the corresponding final THD got with MSOGI (1.7765 %). The final THD is also considerably smaller than the initial THD 2.7772 %.

The SRF based active filter feature is tested also in the maximum capacitive and maximum inductive operations points. Otherwise, the simulation settings are the same but now STATCOM is set to operate at its maximum capacitive operation point. The corresponding harmonic spectrum at PCC before the active filter feature is enabled is similar with the spectrum presented earlier in Figure 34. The final harmonic spectrum at PCC before the active filter control is enabled is shown in Figure 42.

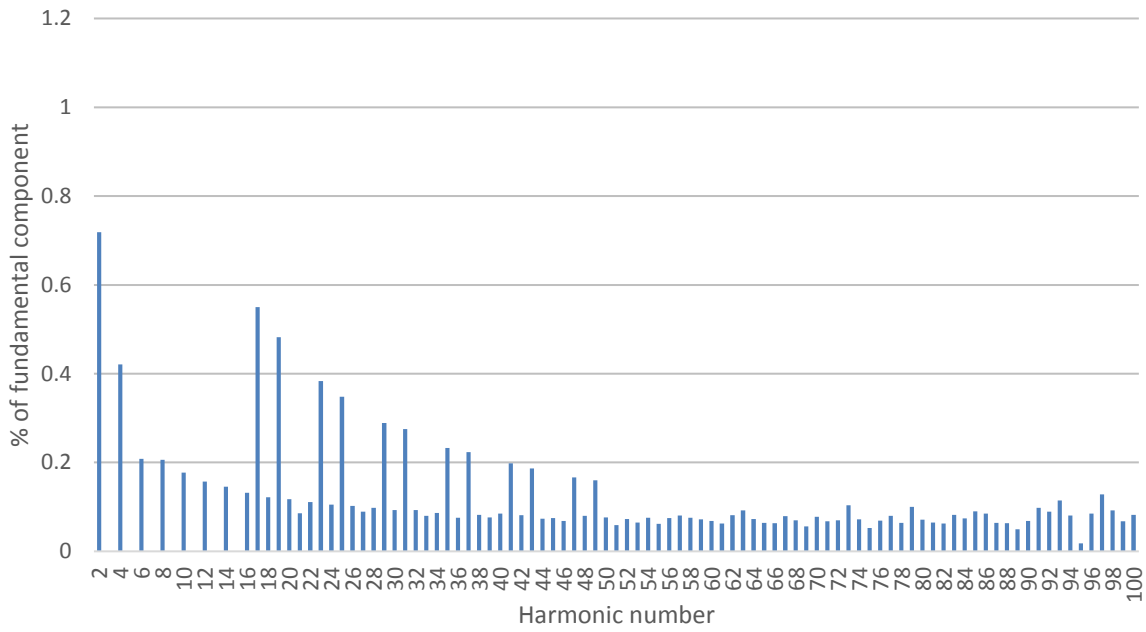


***Figure 42.*** *Harmonics at PCC in case of STATCOM operating at its maximum capacitive operation point and the SRF based active filter is in use.*

As can be seen in Figure 42, the controlled harmonics decrease to zero. Similar to the previous simulation, the harmonic compensation performance remains high even when the grid contains a great number of other harmonics. Moreover, no significant increase in other harmonics can be noticed. Due to the operation at STATCOM's maximum capacitive operation point, the harmonics are smaller in terms of percentage compared to the values got when STATCOM was operated at its zero-operation point. The final THD at PCC settles down to 1.5940 % which is again slightly smaller than the final THD got with MSOGI (1.6773 %) and thus also considerably smaller than the initial THD at PCC (2.6342 %).

Finally, the SRF based active filter feature is tested when STATCOM is set to operate at its maximum inductive operation point. The corresponding harmonic spectrum at PCC before the active filter control is enabled is similar with the harmonic spectrum presented earlier in Figure 37. The final harmonic spectrum at PCC after the active filter control is given enough time to control the grid harmonics to the smallest possible is shown in Figure 43.

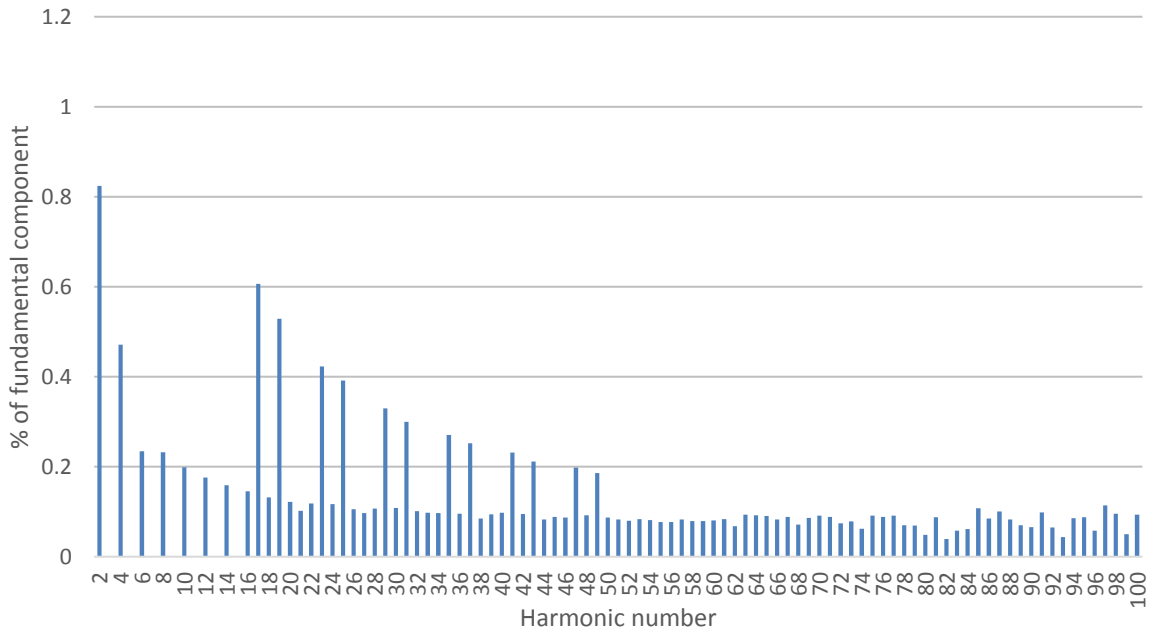


***Figure 43.*** *Harmonics at PCC in case of STATCOM operating at its maximum inductive operation point and the SRF based active filter is in use.*

The controlled harmonics decrease very close to zero also when STATCOM is operated at its maximum inductive operation point as can be noticed in Figure 43. The impact to uncontrolled harmonics is almost negligible but due to STATCOM's operation at its maximum inductive operation point the harmonics are greater in terms of percentage of the fundamental component compared to operations in the capacitive and zero-operation points. The final THD at PCC settles down to 1.7789 % which is smaller than MSOGI's corresponding THD (1.8679 %) and also considerably smaller than the initial THD at PCC (2.9376 %)

As a result, the SRF based active filter feature seems to perform similarly in all three, zero, capacitive and inductive, operation points. The controlled harmonics decrease practically to zero in every case simulated and the difference in performances between the SRF based method and the MSOGI based method especially in terms of final harmonic component values can be considered negligible.

## 5.4 Capacitive grid impedance

In the simulations done in 5.2 and in 5.3 the grid impedance was assumed to be highly inductive. Based on this assumption, corresponding phase shifts were implemented for the reference vector in the control system. As a consequence, if the grid impedance occurs to be capacitive at a certain harmonic frequency, the phase shifts done in the control system wouldn't be correct anymore and thus the active filter feature would start to amplify that particular harmonic component instead of mitigating it. If the grid impedance is

known, the active filter control can be tuned in a way to achieve an optimal performance even if the grid occurs to be capacitive.

The next simulation is done in order to demonstrate that harmonics can be compensated also if the grid impedance occurs to be capacitive. The active filtering is done with the studied MSOGI based method. In the simulation, a highly capacitive grid impedance is assumed and thus the reference vector phase shift is changed in the control system to obtain harmonics compensation correspondingly in the capacitive grid. With capacitive grid, the grid impedance decreases as a function of increasing frequency. If the capacitive grid impedance at the fundamental frequency is set equal with the grid impedance in case of inductive grid, grid impedances at harmonic frequencies would differ a lot. Moreover, the VSC current would need to be enormous to achieve great enough voltage change in in the grid to cancel out the grid harmonics. Thus, the grid impedance is set in a way that it is the same order of magnitude at the 3rd and 5th harmonic as it was in the case of inductive grid. Consequently, the harmonic voltage source in the grid is set to only generate positive sequence components of 3rd and 5th harmonic according to Table 3. Moreover, STATCOM is set to operate at its zero-operation point. The corresponding harmonic spectrum at PCC before the active filter control is enabled is presented in Figure 44.

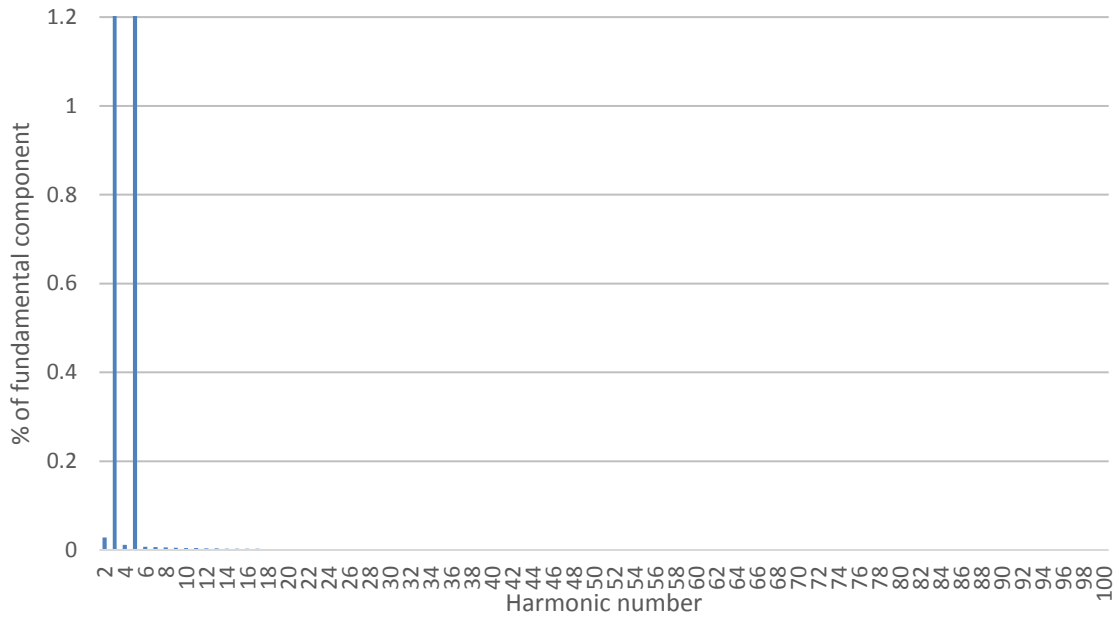


***Figure 44.*** *Harmonic spectrum at PCC when the grid is highly capacitive and the MSOGI based active filter is not in use.*

THD at PCC before harmonic control is enabled is 2.8043 %. The fifth harmonic component is slightly greater than the third harmonic due to the capacitive grid impedance. The harmonic spectrum after the active filter has controlled the grid harmonics to the smallest possible is presented in Figure 45.

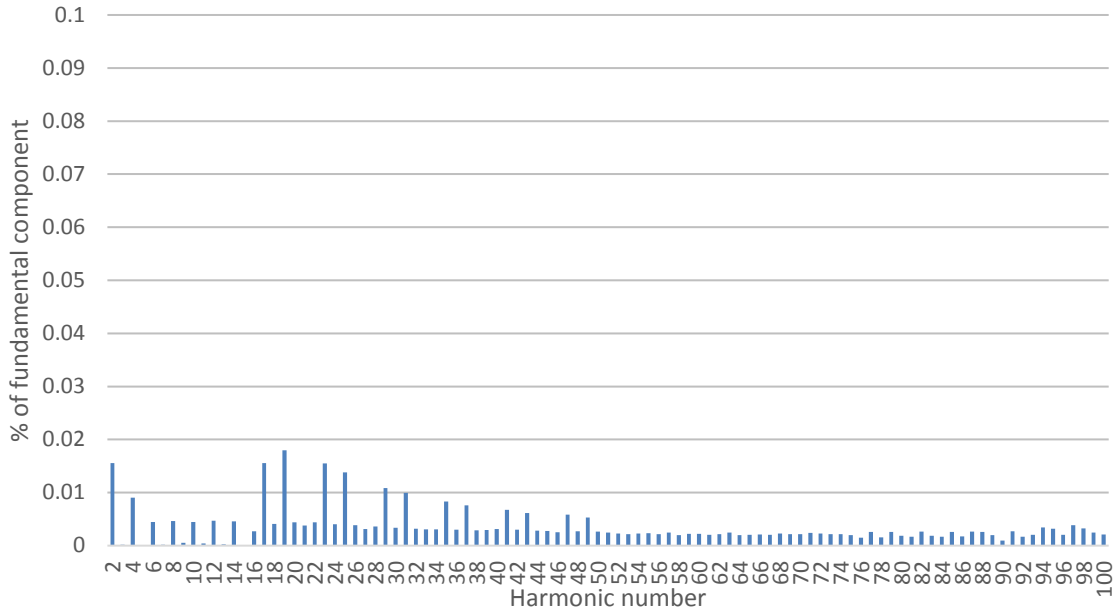


***Figure 45.*** *Harmonic spectrum at PCC when the grid is highly capacitive and the MSOGI based active filter is in use.*

As can be seen in Figure 45, both harmonics, 3rd and 5th, settle down to zero. Even if some variety in other harmonics may be seen, no significant increase in individual harmonic components is still noticed. THD at PCC settles down very close to zero with the final value of 0.0493 %.

As a result, it can be stated that the active harmonic filter works also in case of capacitive grid. However, the grid impedance needs to be known or alternatively the control needs to be designed in order to figure out if the grid occurs to be capacitive at certain harmonic frequencies and further the corresponding phase shifts need to be implemented. If the grid is assumed to be highly inductive and no additional control is designed to recognize capacitive grid impedance, the active filter may start to amplify harmonics instead of compensating them.

# 6. ANALYSIS AND COMPARISON OF THE RESULTS

Simulation results show that both of the studied methods, the MSOGI based method and the SRF based method, are capable of compensating both positive and negative sequence harmonics completely when the grid contains only harmonics STATCOM is set to compensate. Both methods are also capable of compensating harmonics in STATCOM's all three operation points even when the grid contains a great number of other harmonics. The difference in performances between the studied two methods in terms of final controlled harmonic component values is negligible and thus both methods can be considered to be able to compensate harmonics practically completely in steady-state. In terms of final THD values, the SRF based method shows slightly better performance over the MSOGI based method. If an ideal final THD was calculated from the initial situation so that all controlled harmonics would completely decrease to zero and other harmonics wouldn't be affected, the final THD would be for example in case of zero-operation 1.6842 %. The corresponding final THD got with the SRF based method reaches almost the ideal case with 1.6895 %. However, the SRF based method still strengthens some uncontrolled harmonics but at the same time decreases others in a balanced way. The pattern of decreased and strengthened uncontrolled harmonics is rather scattered and no clear rule can be found. Even though the performance of the MSOGI based method in terms of final controlled harmonics values is practically equal with the corresponding performance with the SRF based method, the final THD values (1.7765 % in zero-operation case) do not reach as ideal values as the SRF based method. In other words, the MSOGI based method strengthens a greater number of other harmonics, yet still individual harmonics are not strengthened significantly. Especially harmonics between $20^{th}$ and $50^{th}$ order are strengthened systematically in all STATCOM's operation points. After $50^{th}$ harmonic the pattern of compensated and strengthened harmonics is rather scattered. All in all, based on these simulations, the SRF based active filter method can be considered to have a better performance under steady-state circumstances but the difference is rather insignificant.

A major difference between the two studied methods is the reference frame where each method operates. In the MSOGI based method this reference frame is a stationary reference frame. Since the reference frame is a stationary one whilst the measured grid signals are sinusoidal, the control signals of this control system are thus also sinusoidal. This further causes challenges for the control design as the use of for example conventional PI-controllers is not possible. Moreover, for instance, as the active filter feature is meant to operate simultaneously with the reactive power compensation and as the VSC maximum current must not be exceeded, a control to decrease harmonics compensation when STATCOM already operates close to its maximum reactive power operation points must

be implemented. However, as the reference frame is a stationary one, harmonics can't be easily controlled to a certain value differing from zero with the help of DC reference values to decrease the level of harmonics compensation. Respectively, the SRF based method operates in the synchronous reference frame. Since the reference frame is a rotating one and the measured signals are sinusoidal, the control can be implemented using constant DC values and PI-controllers. As mentioned earlier, this is the conventional way to implement control and the example case of the VSC overcurrent limitation will thus also be simpler to implement. Furthermore, dq-theory is widely used and there exist plenty of literature dealing with the synchronous reference frame control design. All in all, extending and modifying of the active filter feature or anything else related to control design is much more challenging to be carried out in the stationary reference frame than in the synchronous reference frame. Therefore, from the reference frame and control perspective the SRF based method has a considerable advantage over the MSOGI based method.

The possibility for selective harmonics detection and compensation was considered as a mandatory feature to make it even possible to implement the active filter feature in the studied STATCOM system. Both methods are capable of selective harmonics detection and compensation. Moreover, it is rather easy to increase or decrease the number of controlled harmonics i.e. to set the harmonics to be compensated in both cases. In the MSOGI based method increasing or decreasing the number of SOGI blocks affects automatically also on the other SOGI blocks through the cross-feedback network. However, for the both studied methods setting the harmonics to be compensated can be considered as rather simple task. Furthermore, the implementation of the phase shift to neutralize the effects of transformer's and STATCOM's delta-connections as well as the effect of the grid impedance's angle is rather simple to carry out in both methods studied. Anyhow, as the implementation of the control is overall simpler in the synchronous reference frame, also the phase shift implementation can be done with less mathematical operations in the SRF based method.

A major benefit with the MSOGI based method is its potentiality to be used in both three-phase and single-phase applications. This makes it possible to offer the active filter feature regardless whether the project is three-phase, two-phase or single-phase application. Thus, when the control related to the active filter feature is further developed the whole design doesn't need to be redesigned if future projects occur to be for example single-phase projects instead of traditional three-phase projects. This kind of flexibility can be considered as a remarkable advantage especially because the projects can be assumed to become more and more unique and complex in the future. Respectively, the studied SRF based method is capable to only operate in three-phase applications which thus can be considered a major shortcoming. On the other hand, a major part of the projects are still three-phase applications which thus makes it anyway possible to offer active filter feature

to most of the projects even if done with the SRF based method. Nevertheless, this flexibility of the MSOGI based method can be considered a major advantage over the studied SRF based method especially when considering the possible future needs.

All in all, Table 4 presents a comparison of the main characteristics of the SRF and MSOGI based methods.

***Table 4.*** *Comparison of the studied methods.*

| Method | Harmonic dq-frame (SRF) | MSOGI |
|---|---|---|
| Single-phase/Three-phase applications | 3ph | 3ph/1ph |
| Reference frame | Synchronous reference frame | Stationary reference frame |
| Positive sequence harmonics filtering | ++ | ++ |
| Negative sequence harmonics filtering | ++ | ++ |
| Performance under distorted conditions | ++ | + |
| Selective harmonic compensation | Yes | Yes |
| Control design | + | - |
| Expandable | Yes | Yes |
| Dynamic performance | N/A | N/A |

As can be seen in Table 4, the difference in dynamic performances remains still not tested. It can however be assumed that due to MSOGI's cross-feedback network the dynamic performance of the MSOGI based method could be advanced compared to the SRF based method whose dynamics are reduced by the use of low-pass filters. However, in general, harmonics compensation in steady-state can be considered to be enough as harmonics are usually measured and limited mostly as average values. Overall, the studied SRF based method is superior especially from the control design perspective compared to the MSOGI based method. If projects are assumed to be normal three-phase applications in the future, then the SRF based method should be further developed. Consequently, if the suitability also to other than three-phase applications is highly valued, then the MSOGI based method can be considered superior.

# 7. FUTURE STUDY AND DEVELOPMENT NEEDS

In this thesis, two harmonics compensations methods with grid synchronization features were studied. The simulations were done as a proof-of-concept in order to demonstrate the feasibility of the studied methods. Both methods were able to compensate harmonics completely in all three operations points simulated even when the grid contained a great number of other harmonics. In this thesis, steady-state operation was assumed with no transient changes in power flow or voltage due to load or generation changes. The next step in development of the active filter feature would be to carry out simulations to show the performance of the studied methods under dynamic/transient situations. Moreover, a discrete implementation of the studied methods should be done as the control is placed in microprocessors in real life and thus the current active filter models using continuously changing variables may give too optimistic results.

As it was mentioned before, in this thesis, highly inductive grid impedance was assumed and thus the corresponding phase shifts were done in the control system. However, if the grid impedance occurs to be capacitive at some harmonic frequency the active harmonic filter control will start to amplify the particular grid harmonic. In other words, a method for the grid impedance detection is needed. In [31] an identification of grid impedance for purposes of voltage feedback active filtering is presented. The main idea is to measure voltage and current vectors' changes in the grid (at PCC) when a certain harmonic current is injected to the grid. As a result, the grid impedance vector at this certain harmonic frequency can be calculated and thus the correct phase shift can be done for the reference vector in the control system. Based on [31], a grid impedance identification method could be studied, developed and further implemented in the control system to guarantee that harmonics will be compensated even when the grid impedance is not highly inductive. The method should give the correct grid impedance angle, not just 90 or -90 degrees, which thus could improve especially dynamic performance of the active filter feature.

The adaptability of the control to different projects and scenarios can be considered as a major feature. As mentioned in chapter 4.1, one of the major strengths with the MSOGI based method is that it can be easily modified to be used in both three-phase and single-phase applications whereas the studied harmonic dq-frame based method can only be used for three-phase applications. However, with MSOGI the implementation of the control in stationary reference frame can be considered more challenging than the corresponding control in synchronous reference frame with the harmonic dq-frame based method. Recently, some new publications concerning dq-theory based single phase fundamental component control have been published [32, 33]. Consequently, these new methods could be considered and their suitability for harmonics detection and compensation could be

further studied thus possibly enabling the use of harmonic dq-frame also in single-phase applications.

In this thesis, harmonics compensation was set for odd harmonics up to $15^{th}$ harmonic order. In the simulation environment, even higher order harmonics could have been detected and further compensated. However, in practice, for example measuring equipment present a certain error and may not be accurate enough especially to higher order harmonics in high voltage applications. Thus, it will be possible to detect and compensate harmonics accurately only up to a certain harmonic order. Future studies could therefore investigate how many harmonics can actually be compensated in practice. Furthermore, measuring instrument present certain transfer functions which thus could be used to model the effect of measuring instrument to measured signal and as a consequence it could be taken into account to achieve accurate measurements and further to enable even higher order harmonics compensation. The compensation of higher order harmonics may also cause challenges for the STATCOM dimensioning as for example harmonic current of $9^{th}$ order causes 9 times greater voltage across the VSC's coupling coil compared to the corresponding fundamental current. If a great amount of higher order harmonics is to be compensated simultaneously with the reactive power compensation, the number of VSC submodules needs to be increased.

# 8. CONCLUSIONS

The purpose of this thesis was to study and simulate different methods for active harmonic filtering to be used as an add-on feature on a reactive power compensation system STATCOM. Two harmonics compensation methods with grid synchronization features were studied comprehensively and further simulated in PSCAD environment in order to demonstrate their feasibilities as a proof-of-concept. The simulations were done assuming a steady-state operation and no simulations were done at this point to illustrate the dynamic behavior of the studied methods.

Both methods, the MSOGI based active filter method and the SRF based active filter method, were able to compensate harmonics' positive and negative sequence components completely when the grid contained only harmonics STATCOM was set to compensate. Further simulations showed that both methods were as well able to compensate harmonics in STATCOM's all three operation points (zero-operation, the maximum capacitive and the maximum inductive) to zero even when the grid contained a great number of other harmonics. Moreover, neither of the studied methods significantly strengthened individual uncontrolled harmonics in the grid as was desired. The difference in performances between the studied two methods in terms of final controlled harmonic component values was negligible. On the other hand, the SRF based method had less adverse effect on uncontrolled harmonics which resulted in better performance in terms of final voltage THD values compared to the MSOGI based method. However, the difference in the final results between the MSOGI and SRF based methods is overall rather insignificant and both methods can be considered to perform properly in steady-state case.

A major benefit in the MSOGI based active filter method is its potentiality to be used in both three-phase and single-phase applications. This can be considered as a remarkable advantage as projects vary from conventional three-phase applications all the way to single-phase and even more and more complex applications. This flexibility makes it thus possible to offer the active filter feature to most of the projects. On the other hand, MSOGI operates in the stationary reference frame, not in the conventional synchronous reference frame (dq-frame), which therefore makes the control design more complex. In contrast, the SRF based method operates in the synchronous reference frame and thus has the advantage to implement control using DC values and conventional PI-controllers. Moreover, dq-theory is widely used in control systems and thus the SRF based method has also the advantage of well-covered literature. However, the current studied SRF based method is capable to work only in three-phase applications which can be considered a major shortcoming.

Dynamic performances of the studied methods were not tested in this thesis. However, as in general terms the ability to compensate harmonics in steady-state operation can be

considered to be enough and as both methods perform properly under steady-state conditions, the choice of the active filter method depends on external issues. All in all, if future studies show the possibility for SRF based method to be used also in single-phase applications or if a high number of future projects is assumed to be conventional three-phase applications, then the SRF based method should be further developed. Consequently, if the ability to be easily modified to both three-phase and single-phase applications is highly valued, then the MSOGI based method can be considered superior based on this thesis.

# REFERENCES

[1] F. De La Rosa, Harmonics and power systems, Taylor & Francis, Boca Raton, Fla., 2006, 1-179 p.

[2] H. Akagi, Active Harmonic Filters, Proceedings of the IEEE, Vol. 93, Iss. 12, 2005, pp. 2128-2141.

[3] CIGRE Working Group 14.19, Static Synchronous Compensator (STATCOM), CIRGE, 2000, 211 p.

[4] F.T. Ghetti, A.A. Ferreira, H.A.C. Braga, P.G. Barbosa, A study of shunt active power filter based on modular multilevel converter (MMC), 10th IEEE/IAS International Conference on Industry Applications, 2012, pp. 1-6.

[5] F. BasheerAldousari, Power System Harmonics, International Journal of Engineering Research and Applications, Vol. 6, Iss. 10, 2016, pp. 55-61.

[6] IEEE 519, Recommended Practice and Requirements for Harmonic Control in Electric Power Systems, IEEE, The Institute of Electrical and Electronics Engineers, 2014, pp. 100.

[7] O. Al-duaij, Harmonics Effects in Power System, International Journal of Engineering Research and Applications, Vol. 5, Iss. 2, 2015, pp. 1-19.

[8] H. Asgharpour-Alamdari, Y. Alinejad-Beromi, H. Yaghobi, Reduction in distortion of the synchronous generator voltage waveform using a new winding pattern, IET Electric Power Applications, Vol. 11, Iss. 2, 2017, pp. 233-241.

[9] R. Snehal, D. Dnyaneshwar, A Review of Harmonics Detection and Measurement in Power System, International Journal of Computer Applications, Vol. 143, Iss. 10, 2016, pp. 42-45.

[10] G. Ajenikoko, A. Ojerinde, Effects of Total Harmonic Distortion on Power System Equipment, Vol. 6, 2015, pp. 114-121.

[11] F.A. Benson, Skin effect (electricity), Access Science, 2014. Available in [referred 12.11.2017]: http://accessscience.com.libproxy.tut.fi/content/skin-effect-electricity/627200.

[12] T.S. Key, J. Lai, Costs and Benefits of Harmonic Current Reduction for Switch-Mode Power Supplies in a Commercial Office Building, IEEE Transactions on Industry Applications, Vol. 32, Iss. 5, 1996, pp. 1017-1025.

[13] CIGRE Working Group 14.30, Guide to the specification and design evaluation of a.c. filters for HVDC systems, 1999.

[14] V. Cuk, J.F.G. Cobben, P.F. Ribeiro, W.L. Kling, J.F.G. Cobben, P.F. Ribeiro, A review of international limits for harmonic voltages and currents in public networks, 16th International Conference on Harmonics and Quality of Power (ICHQP), 2014, pp. 621-625.

[15] S.M. Halpin, Comparison of IEEE and IEC harmonic standards, IEEE Power Engineering Society General Meeting, 2005, IEEE, pp. 2214-2216.

[16] G. Benysek, M. Pasko, Power Theories for Improved Power Quality, Springer, 2012, 217 p.

[17] W. Hofmann, J. Schlabbach, W. Just, Reactive Power Compensation: A Practical Guide, 1st ed. Wiley, Hoboken, 2012, pp. 23-35.

[18] A. Baggini, A. Sumper, Electrical Energy Efficiency: Technologies and Applications, 1st ed. John Wiley & Sons, Incorporated, Hoboken, 2012, pp. 371-398.

[19] BS EN 50160, Voltage characteristics of electricity supplied by public electricity networks, British Standards Institute, 2010.

[20] IEC 60038, Standard voltages, IEC, 2009.

[21] J. Dixon, L. Moran, J. Rodriguez, R. Domke, Reactive Power Compensation Technologies: State-of-the-Art Review, Proceedings of the IEEE, Vol. 93, Iss. 12, 2005, pp. 2144-2164.

[22] B Singh, R Saha, A Chandra, K Al-Haddad, Static synchronous compensators (STATCOM): a review, IET Power Electronics, Vol. 2, Iss. 4, 2009, pp. 297.

[23] P. Rodríguez, R. Teodorescu, I. Candela, A.V. Timbus, M. Liserre, F. Blaabjerg, New positive-sequence voltage detector for grid synchronization of power converters under faulty grid conditions, 2006 37th IEEE Power Electronics Specialists Conference, pp. 1-7.

[24] P. Rodriguez, A. Luna, I. Candela, R. Teodorescu, F. Blaabjerg, Grid synchronization of power converters using multiple second order generalized integrators, 34th Annual Conference of IEEE Industrial Electronics, pp. 755-760.

[25] P. Rodriguez, A. Luna, I. Etxeberria, J.R. Hermoso, R. Teodorescu, Multiple second order generalized integrators for harmonic synchronization of power converters, IEEE Energy Conversion Congress and Exposition, 2009, pp. 2239-2246.

[26] N. Tleis, Power Systems Modelling and Fault Analysis: Theory and Practice, Elsevier Science & Technology, Oxford, United Kingdom, 2007, 603 p.

[27] D.P. Kothari, I.J. Nagrath, Modern Power System Analysis, Tata McGraw-Hill Publishing Company Limited, New Delhi, 2003, 694 p.

[28] R. Teodorescu, M. Liserre, P. Rodriguez, F. Blaabjerg, Grid Converters for Photovoltaic and Wind Power Systems, John Wiley & Sons, Incorporated, New York, United Kingdom, 2010, 416 p.

[29] C. Kamble, D. Suryawanshi, R. Humane, Time Domain Method for Harmonic Detection in Active Power Filter, 2015, pp. 153-156.

[30] K. Areerak, Harmonic Detection Algorithm based on DQ Axis with Fourier Analysis for Hybrid Power Filters, Vol. 3, 2008, pp. 665-674.

[31] A. Tarkiainen, R. Pollanen, M. Niemela, J. Pyrhonen, Identification of grid impedance for purposes of voltage feedback active filtering, IEEE Power Electronics Letters, Vol. 2, Iss. 1, 2004, pp. 6-10.

[32] M. Li, Y. Wang, X. Fang, Y. Gao, Z. Wang, A Novel Single Phase Synchronous Reference Frame Phase-Locked Loop with a Constant Zero Orthogonal Component, Journal of Power Electronics, Vol. 14, Iss. 6, 2014, pp. 1334-1344.

[33] D.N. Katole, M.B. Daigavane, S.P. Gawande, P.M. Daigavane, Analysis, Design and Implementation of Single Phase SRF Controller for Dynamic Voltage Restorer under Distorted Supply Condition, Energy Procedia, 2017, pp. 716-723.

# APPENDIX A: SYSTEM PARAMETERS FOR SIMULATIONS

***Appendix A Table 1.*** *System parameters for simulations.*

| Parameter | Value | Unit |
|---|---|---|
| Grid | | |
| System nominal frequency | 50 | Hz |
| System nominal voltage, line-to-line | 138 | kV (RMS) |
| Grid resistance | 0.9292 | Ω |
| Grid reactance (at the fundamental frequency) | 9.477 | Ω |
| Transformer | | |
| Transformer type | YNd11 | - |
| Rated power | 100 | MVA |
| Secondary nominal voltage, line-to-line | 34.5 | kV (RMS) |
| STATCOM | | |
| Rated power | 100 | MVAr |
| Number of submodules in one branch | 40 | - |
| Submodule DC-voltage reference | 1.75 | kV |
| Branch inductance | 11 | mH |
| Inductor resistance | 20 | mΩ |
| Capacitive grid simulation | | |
| Grid resistance | 1 | Ω |
| Grid reactance (at the fundamental frequency) | 150 | Ω |